Electronic Supporting Information

Circularly polarized luminescence induction on a Tb(III) complex with a tris(*o-tert*-butylaryloxide)-functionalized 1,4,7-triazacyclononane ligand coordinating chiral 1-phenylethylamine

Sora Shirai[a], Satoshi Muratsugu*[a], Hisaki Matsui[b], Kazuhiro Harada[b], Masahiro Ehara[c], Hidetaka Nakai*[b] and Mizuki Tada*[a]

[a] Department of Chemistry, Graduate School of Science/Integrated Research Consortium on Chemical Science/Research Center for Materials Science, Nagoya University, Furo-cho, Chikusa-ku, Nagoya, 464-8602, Aichi, Japan.
[b] Department of Energy and Materials, Faculty of Science and Engineering/Graduate School of Science and Engineering, 3-4-1 Kowakae, Higashi-Osaka, Osaka, 577-8502, Japan.
[c] Institute for Molecular Science/School of Physical Sciences, Graduate University for Advanced Studies, Myodaiji, Okazaki, 444-8585, Aichi, Japan.

E-mail: muratsugu.satoshi.a5@f.mail.nagoya-u.ac.jp, nakai@emat.kindai.ac.jp, tada.mizuki.u6@f.mail.nagoya-u.ac.jp

1. Molecular structures

$^{t\mathrm{Bu}}\mathbf{1}_{\mathbf{Tb}}$: {($^{t\mathrm{BuMe}}$ArO)$_3$tacn}Tb$^{\mathrm{III}}$(DMF)

$^{t\mathrm{Bu}}\mathbf{1}_{\mathbf{Tb}}'$: {($^{t\mathrm{BuMe}}$ArO)$_3$tacn}Tb$^{\mathrm{III}}$ unit

$^{\mathrm{Me}}\mathbf{1}_{\mathbf{Tb}}$: {($^{\mathrm{MeMe}}$ArO)$_3$tacn}Tb$^{\mathrm{III}}$(THF)

$^{\mathrm{Me}}\mathbf{1}_{\mathbf{Tb}}'$: {($^{\mathrm{MeMe}}$ArO)$_3$tacn}Tb$^{\mathrm{III}}$ unit

$^{t\mathrm{Bu}}\mathbf{1}_{\mathbf{Y}}$: {($^{t\mathrm{BuMe}}$ArO)$_3$tacn}Y$^{\mathrm{III}}$(DMF)

$\mathbf{L}_{\mathbf{NH2}}$: 1-phenylethylamine

$\mathbf{L}_{\mathbf{OH}}$: 1-phenylethyl alcohol

$\mathbf{L}_{\mathbf{NHAc}}$: *N*-(1-phenylethyl)acetamide

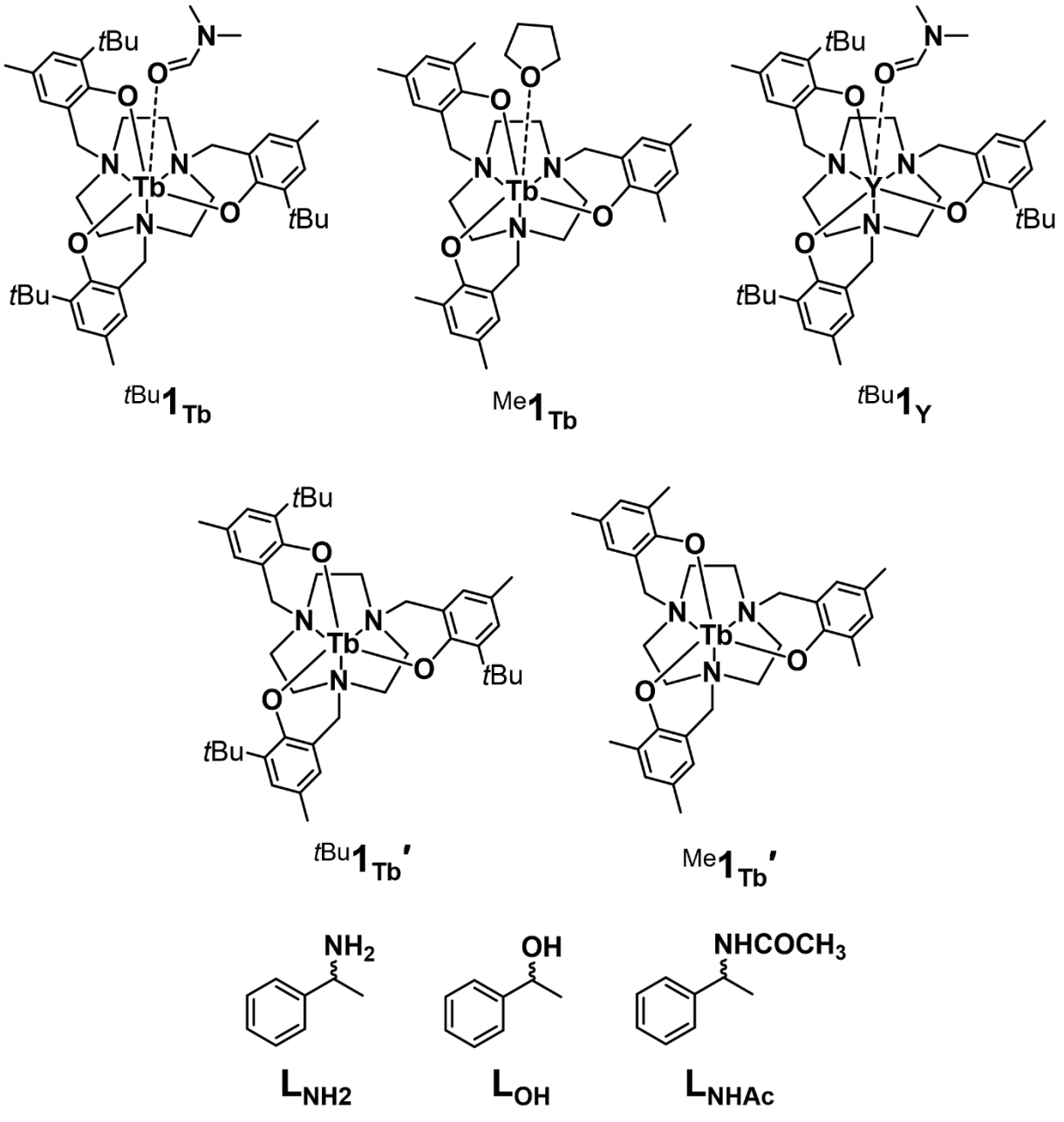

Scheme S1 Molecular structures used in this paper.

2. Experimental Section

2-1. Materials and instruments

All experimental works were performed in an Ar-filled glovebox or in standard Schlenk tubes under an N_2 atmosphere. Chemicals were purchased from commercial sources (Wako Chemicals, TCI, Sigma-Aldrich, or Kishida Reagents Chemicals) and used without further purification unless otherwise noted. Solvents of super dehydrated grade (dimethylformamide (DMF), tetrahydrofuran (THF), and *n*-hexane) were purchased from Wako Chemicals and used as received. Triethylamine (Et_3N) was dried over CaH_2 before use.

Triazacyclononane trihydrochlorate and $^{Me}\mathbf{1_{Tb}}$ were prepared according to the literatures.[1,2] Triazacyclononane and 1,4,7-tris(3-*tert*-butyl-2-hydroxide-5-methylbenzyl)-1,4,7-triazacyclononane ($(^{tBuMe}ArOH)_3tacn$) were prepared by modified literature methods.[1,3] Chiral molecules, (*R*)- and (*S*)-1-phenylethylamine ($\mathbf{L_{NH2}}$) and (*R*)- and (*S*)-1-phenylethyl alcohol ($\mathbf{L_{OH}}$) were purchased from TCI and used as received. (*R*)- and (*S*)-*N*-(1-phenylethyl)acetamide ($\mathbf{L_{NHAc}}$) were prepared according to the literature.[4]

Elemental analysis was carried out on an elemental analyser (MT-6, YANAKO). FT-IR spectra were measured on an FT-IR spectrometer (FT/IR-4200, JASCO) using KBr plates. THF (super dehydrated grade) was purchased from Wako Chemicals and used as received for spectroscopic experiments.

^{1}H NMR and valuable temperature (VT) ^{1}H NMR was carried out on an NMR spectrometer (ECA600, JEOL).

2-2. Synthesis of {(^{tBuMe}ArO)$_3$tacn}Tb^{III}(DMF) [$^{tBu}\mathbf{1_{Tb}}$]

($^{tBuMe}ArOH)_3tacn$ (1.5 g, 2.3 mmol) and $Tb(OTf)_3$ (1.4 g, 2.3 mmol) in DMF/THF = 10/1 (75 mL) were stirred at 328 K for 1 h. Et_3N (1.1 mL, 8.1 mmol) was added to the mixture, and the mixture was stirred at 328 K for 25 h. The mixture was cooled to 293 K, and the white precipitate was collected by filtration and was recrystallized in THF/*n*-hexane = 1/13 at 293 K to obtain colourless crystals of $^{tBu}\mathbf{1_{Tb}}$ (0.82 g, 0.92 mmol, yield: 40%).

Elemental analysis: calcd. for $^{tBu}\mathbf{1_{Tb}}$ ($C_{45}H_{67}N_4O_4Tb$): C: 60.94; H: 7.61; N: 6.32%. Found: C: 60.86; H: 7.80; N: 6.35%. UV-vis (THF): λ_{max} (ε/L mol^{-1} cm^{-1}) = 301 nm (1.3×10^4). FT-IR (KBr): 1669 cm^{-1} (DMF, C=O stretch).

2-3. Synthesis of {(^{tBuMe}ArO)$_3$tacn}Y^{III}(DMF) [$^{tBu}\mathbf{1_Y}$]

($^{tBuMe}ArOH)_3tacn$ (0.50 g, 0.76 mmol) and $Y(OTf)_3$ (0.41 g, 0.76 mmol) in DMF/THF = 10/1 (25 mL) were stirred at 293 K for 15 min. Et_3N (0.38 mL, 2.7 mmol) was added to the mixture, and the mixture was stirred at 328 K for 24 h. The mixture was cooled to 293 K, and the white precipitate was collected by filtration and was recrystallized in THF/*n*-hexane = 1/10 at 293 K to obtain colorless crystals of $^{tBu}\mathbf{1_Y}$ (0.22 g, 0.27 mmol, yield: 36%).

^{1}H NMR (600 MHz, THF-d_8, 298 K, ppm): δ = 8.04 (s; C*H*O), 6.95 (d, J = 2.3 Hz, 3H; Ar-C*H*-4), 6.64 (d, J = 2.3 Hz, 3H; Ar-C*H*-6), 4.30 (d, J = 11.9 Hz, 3H; CH_2-Ar), 3.08 (d, J = 12.4 Hz, 3H; CH_2-Ar), 2.90 (s; N(CH_3)$_2$), 2.88–2.82 (m, 3H; CH_2-N), 2.80 (s; N(CH_3)$_2$), 2.68–2.62 (m, 6H; CH_2-N), 2.14 (s, 9H; CH_3-Ar), 2.07–2.03 (m, 3H; CH_2-N), 1.43 (s, 27H; C(CH_3)$_3$). Elemental analysis: calcd. for $^{tBu}\mathbf{1_Y}$·0.8H_2O ($C_{45}H_{67}N_4O_4Y$·$H_{1.6}O_{0.8}$): C: 65.01; H: 8.32; N: 6.74%. Found: C: 65.08; H: 8.13; N: 6.46%. FT-IR (KBr): 1670 cm^{-1} (DMF, C=O stretch).

2-4. Preparation of single crystal of {($^{t\mathrm{BuMe}}$ArO)$_3$tacn}Tb$^{\mathrm{III}}$((*R*)-L$_{\mathrm{NH2}}$) [$^{t\mathrm{Bu}}$**1**$_{\mathrm{Tb}}$/(*R*)-L$_{\mathrm{NH2}}$]

$^{t\mathrm{Bu}}$**1**$_{\mathrm{Tb}}$ (10 mg, 0.011 mmol) was dissolved in (*R*)-L$_{\mathrm{NH2}}$ (0.3 mL), and *n*-hexane (5 mL) was added to the solution under Ar at 293 K. Colourless crystals of $^{t\mathrm{Bu}}$**1**$_{\mathrm{Tb}}$/(*R*)-L$_{\mathrm{NH2}}$ formed in the solution, and one of the crystals was used for single-crystal X-ray analysis.

2-5. Single-crystal X-ray diffraction

The single crystal was mounted on a glass loop with liquid paraffin. Diffraction data were collected at 123 K by an X-ray diffractometer (Rigaku) equipped with a microfocus rotating anode X-ray generator (MicroMax-007) by using graphite-monochromated Mo K_α radiation (0.7107 Å) and a hybrid photon counting detector (HyPix6000) under a cold N_2 stream. The frame data were integrated and corrected for absorption with the CrysAlis$^{\mathrm{Pro}}$ package (Rigaku Oxford Diffraction). The diffraction data were analysed by the direct method (SHELXT)[5] and refined by full-matrix least-square procedures on F^2 (SHELXL-2018).[6] All non-hydrogen atoms were refined anisotropically. All hydrogen atoms were placed at the calculated positions and refined using a riding model. All calculations were performed using the Olex2-1.5 software package.[7] The crystallographic data are given in **Table S1**.

2-6. UV-vis spectra and luminescent properties

All experimental works were performed in an Ar-filled glovebox. Solution samples in THF were sealed in quartz cells (1 × 1 cm) under an Ar atmosphere at 293 K. All UV-vis spectra were recorded with a UV-vis spectrometer (V-550, JASCO). Parameters for UV-vis measurements were set as follows; scan rate: 400 nm min^{-1}; data interval: 1 nm; band width: 1 nm; accumulated number: 1.

All photoluminescence (PL) and excitation spectra were recorded with a spectrofluorometer (FP-6600, JASCO). Parameters for PL and excitation measurement were set as follows; scan rate: 200 nm min^{-1}; data interval: 0.4 nm; excitation band width: 5 nm; emission band width: 10 nm; response: 2 s.; accumulated number: 1. The excitation wavelength for PL measurements was 300 nm, and the emission wavelength for excitation measurements was 547 nm.

Luminescence lifetime (τ) and luminescence quantum yield (Φ) were measured with a spectrofluorometer (FluoroMax-4P, Horiba Jobin Yvon), and the measurements were independently repeated at least three times. Luminescence quantum yield (Φ) was measured by the relative comparison method with quinine bisulfate in 0.5 M H_2SO_4 ($\Phi = 0.60$) and $^{\mathrm{Me}}$**1**$_{\mathrm{Tb}}$ in THF ($\Phi = 0.91$) chosen for the standards. Maximum error in the reported value was within ±10% which was confirmed by the cross-calibration of the standard sample.[2,8] The general equation used for the determination of relative quantum yields is given as

$$Q_x/Q_{st} = [A_{st}(\lambda)/A_x(\lambda)][I_x/I_{st}][n_x^2/n_{st}^2] \qquad (1)$$

where A is absorbance at excitation wavelength, I is integrated luminescence intensity, and n is the refractive index. Subscripts x and st represent sample and standard, respectively.[9]

Dissymmetry factor (g_{lum}) was calculated by using an equation given as

$$g_{\mathrm{lum}} = \Delta I / I \qquad (2)$$

where ΔI is intensity difference in left- and right-handed CPL, and I is total luminescence intensity.[10]

CPL brightness (B_{CPL}) was calculated for the selected f-f transition of lanthanide complex by using an equation given as

$$B_{CPL} = \beta_i \times \varepsilon_\lambda \times \Phi \times |g_{lum}|/2 \qquad (3)$$

where ε_λ is molar extinction coefficient at the excitation wavelength (λ). β_i is branching ratio given by $\beta_i = I_i / \Sigma_j I_j$, where I_i is the integrated luminescence intensity of considered f-f transition, and $\Sigma_j I_j$ is the summation of the integrated luminescence intensities over all the transitions.[11]

2-7. Circularly polarized luminescence spectra

All experimental works were performed in an Ar-filled glovebox. Sample solutions of $^{t\mathrm{Bu}}\mathbf{1_{Tb}}/^{\mathrm{Me}}\mathbf{1_{Tb}}$ in THF ($[^{t\mathrm{Bu}}\mathbf{1_{Tb}}/^{\mathrm{Me}}\mathbf{1_{Tb}}] = 1 \times 10^{-3}$ mol L^{-1}) and a chiral ligand ((*R*)- or (*S*)-$\mathbf{L_{NH2}}$, $\mathbf{L_{OH}}$, or $\mathbf{L_{NHAc}}$) for circularly polarized luminescence (CPL) measurements were sealed in quartz cells (1 × 1 cm) under an Ar atmosphere at 293 K. The neat solution samples of $^{t\mathrm{Bu}}\mathbf{1_{Tb}}/^{\mathrm{Me}}\mathbf{1_{Tb}}$ in (*R*)- or (*S*)-$\mathbf{L_{NH2}}$ ($[^{t\mathrm{Bu}}\mathbf{1_{Tb}}/^{\mathrm{Me}}\mathbf{1_{Tb}}] = 4 \times 10^{-3}$ mol L^{-1}) were prepared and sealed in quartz cells (1 × 0.1 cm) under an Ar atmosphere at 293 K. All CPL spectra were recorded with a CPL spectrometer (CPL-300, JASCO). Parameters for CPL measurement were set as follows; excitation wavelength: 300 nm; scan rate: 50 nm min^{-1}; data interval: 0.5 nm; excitation band width: 10 nm; emission band width: 10 nm; response: 8 s.; accumulated number: 2.

3. Computational details

All ground-state calculations were conducted using density functional theory with dispersion correction (DFT-D3)[12] and the B3LYP functional.[13] ECP46MWB[14] and ECP54MWB[14] were employed for the lanthanum (La) and terbium (Tb) atoms, respectively, and the 6-31G(d)[15] basis set was used for the other atoms. The solvent effect of THF was included by using the SMD approach with the solvent-accessible surface (SAS) area model.[16,17] All calculations were performed by using the Gaussian 16 Rev. A.03[18] and Rev. C.02[18] suite of programs. Molecular structures were visualized by using the GaussView 6.0 software[19] and Mercury 2022.1.0.

3-1. Optimized structures of $^{t\mathrm{Bu}}\mathbf{1}_{\mathbf{Tb}}$ and $^{\mathrm{Me}}\mathbf{1}_{\mathbf{Tb}}$ units coordinated with (*R*)- or (*S*)-$\mathbf{L}_{\mathbf{NH2}}$ [$^{t\mathrm{Bu}}\mathbf{1}_{\mathbf{Tb}}$/(*R*)- or (*S*)-$\mathbf{L}_{\mathbf{NH2}}$ and $^{\mathrm{Me}}\mathbf{1}_{\mathbf{Tb}}$/(*R*)- or (*S*)-$\mathbf{L}_{\mathbf{NH2}}$]

The structures of $^{t\mathrm{Bu}}\mathbf{1}_{\mathbf{Tb}}$/(*R*)- or (*S*)-$\mathbf{L}_{\mathbf{NH2}}$ and $^{\mathrm{Me}}\mathbf{1}_{\mathbf{Tb}}$/(*R*)- or (*S*)-$\mathbf{L}_{\mathbf{NH2}}$ were optimized by sequences shown in **Scheme S2**. To reduce the computational costs, the Tb centre (septet) of an initial structure made from a single crystal structure of $^{\mathrm{Me}}\mathbf{1}_{\mathbf{Tb}}$[2] was replaced with a La centre (singlet), and geometry optimization was performed. After the structure was optimized, the La centre was changed to a Tb centre, and further geometry optimization was performed. All calculations were conducted for both *Δ*- and *Λ*-isomers of $^{t\mathrm{Bu}}\mathbf{1}_{\mathbf{Tb}}$/(*R*)- or (*S*)-$\mathbf{L}_{\mathbf{NH2}}$ and $^{\mathrm{Me}}\mathbf{1}_{\mathbf{Tb}}$/(*R*)- or (*S*)-$\mathbf{L}_{\mathbf{NH2}}$. Calculated total energies are listed in **Tables S4** and **S5**.

Step 1: Optimized structure of [{($^{\mathrm{MeMe}}$ArO)$_3$tacn}La$^{\mathrm{III}}$((*S*)-$\mathbf{L}_{\mathbf{OH}}$)] ($^{\mathrm{Me}}\mathbf{1}_{\mathbf{La}}$/(*S*)-$\mathbf{L}_{\mathbf{OH}}$)

An optimized structure of [{($^{\mathrm{MeMe}}$ArO)$_3$tacn}La$^{\mathrm{III}}$((*S*)-$\mathbf{L}_{\mathbf{OH}}$)] (denoted as $^{\mathrm{Me}}\mathbf{1}_{\mathbf{La}}$/(*S*)-$\mathbf{L}_{\mathbf{OH}}$) was calculated to determine the configuration of the 1-phenylethyl group. The initial molecular structures of $^{\mathrm{Me}}\mathbf{1}_{\mathbf{Tb}}$ were extracted from the single-crystal structure of $^{\mathrm{Me}}\mathbf{1}_{\mathbf{Tb}}$,[2] and the Tb$^{\mathrm{III}}$ centre (septet) was changed to a La$^{\mathrm{III}}$ (singlet) atom and THF was changed to (*S*)-$\mathbf{L}_{\mathbf{OH}}$. The position of the O atom of (*S*)-$\mathbf{L}_{\mathbf{NH2}}$ was set to that of coordinated THF.

Step 2-Me: Optimized structure of [{($^{\mathrm{MeMe}}$ArO)$_3$tacn}La$^{\mathrm{III}}$((*S*)-$\mathbf{L}_{\mathbf{NH2}}$)] ($^{\mathrm{Me}}\mathbf{1}_{\mathbf{La}}$/(*S*)-$\mathbf{L}_{\mathbf{NH2}}$)

An optimized structure of [{($^{\mathrm{MeMe}}$ArO)$_3$tacn}La$^{\mathrm{III}}$((*S*)-$\mathbf{L}_{\mathbf{NH2}}$)] (denoted as $^{\mathrm{Me}}\mathbf{1}_{\mathbf{La}}$/(*S*)-$\mathbf{L}_{\mathbf{NH2}}$) was calculated to determine the structure of the {($^{\mathrm{MeMe}}$ArO)$_3$tacn}$^{3-}$ ligand and (*S*)-$\mathbf{L}_{\mathbf{NH2}}$. An initial structure was created from the optimized structure of $^{\mathrm{Me}}\mathbf{1}_{\mathbf{La}}$/(*S*)-$\mathbf{L}_{\mathbf{OH}}$ by changing the OH group of coordinated (*S*)-$\mathbf{L}_{\mathbf{OH}}$ to an NH_2 group.

Step 3-Me: Optimized structure of [{($^{\mathrm{MeMe}}$ArO)$_3$tacn}Tb$^{\mathrm{III}}$((*S*)-$\mathbf{L}_{\mathbf{NH2}}$)] ($^{\mathrm{Me}}\mathbf{1}_{\mathbf{Tb}}$/(*S*)-$\mathbf{L}_{\mathbf{NH2}}$)

One of the target optimized structures, [{($^{\mathrm{MeMe}}$ArO)$_3$tacn}Tb$^{\mathrm{III}}$((*S*)-$\mathbf{L}_{\mathbf{NH2}}$)] (denoted as $^{\mathrm{Me}}\mathbf{1}_{\mathbf{Tb}}$/(*S*)-$\mathbf{L}_{\mathbf{NH2}}$), was calculated. An initial structure was created from the optimized structure of $^{\mathrm{Me}}\mathbf{1}_{\mathbf{La}}$/(*S*)-$\mathbf{L}_{\mathbf{NH2}}$ by replacing its La$^{\mathrm{III}}$ centre with a Tb$^{\mathrm{III}}$ atom.

Step 4-Me: Optimized structure of [{($^{\mathrm{MeMe}}$ArO)$_3$tacn}Tb$^{\mathrm{III}}$((*R*)-$\mathbf{L}_{\mathbf{NH2}}$)] [$^{\mathrm{Me}}\mathbf{1}_{\mathbf{Tb}}$/(*R*)-$\mathbf{L}_{\mathbf{NH2}}$]

One of the target optimized structures, [{($^{\mathrm{MeMe}}$ArO)$_3$tacn}Tb$^{\mathrm{III}}$((*R*)-$\mathbf{L}_{\mathbf{NH2}}$)] (denoted as $^{\mathrm{Me}}\mathbf{1}_{\mathbf{Tb}}$/(*R*)-$\mathbf{L}_{\mathbf{NH2}}$) was calculated. An initial structure was created by mirror inversion of the optimized structure of $^{\mathrm{Me}}\mathbf{1}_{\mathbf{Tb}}$/(*S*)-$\mathbf{L}_{\mathbf{NH2}}$.

Step 2-*t*Bu: Optimized structure of [{($^{t\mathrm{BuMe}}$ArO)$_3$tacn}La$^{\mathrm{III}}$((*S*)-$\mathbf{L}_{\mathbf{NH2}}$)] [$^{t\mathrm{Bu}}\mathbf{1}_{\mathbf{La}}$/(*S*)-$\mathbf{L}_{\mathbf{NH2}}$]

An optimized structure of [{($^{t\mathrm{BuMe}}$ArO)$_3$tacn}La$^{\mathrm{III}}$((*S*)-$\mathbf{L}_{\mathbf{NH2}}$)] (denoted as $^{t\mathrm{Bu}}\mathbf{1}_{\mathbf{La}}$/(*S*)-$\mathbf{L}_{\mathbf{NH2}}$) was calculated to determine the structure of {($^{t\mathrm{BuMe}}$ArO)$_3$tacn}$^{3-}$ ligand and (*S*)-$\mathbf{L}_{\mathbf{NH2}}$. An initial structure was created from

^{Me}**1$_{La}$**/(*S*)-**L$_{OH}$** by changing the methyl groups at the *ortho*-position of the phenoxide moieties to *tert*-butyl groups, and the OH group of (*S*)-**L$_{NH2}$** to an NH_2 group.

Step 3-*t*Bu: Optimized structure of [{(^{t}BuMeArO)$_3$tacn}Tb^{III}((*S*)-**L$_{NH2}$**)] [^{tBu}**1$_{Tb}$**/(*S*)-**L$_{NH2}$**]

One of the target optimized structures, [{(^{t}BuMeArO)$_3$tacn}Tb^{III}((*S*)-**L$_{NH2}$**)] (denoted as ^{tBu}**1$_{Tb}$**/(*S*)-**L$_{NH2}$**), was calculated. An initial structure was created from the optimized structure of ^{tBu}**1$_{La}$**/(*S*)-**L$_{NH2}$** by replacing its La^{III} centre with a Tb^{III} atom.

Step 4-*t*Bu: Optimized structure of [{(^{t}BuMeArO)$_3$tacn}Tb^{III}((*R*)-**L$_{NH2}$**)] [^{tBu}**1$_{Tb}$**/(*R*)-**L$_{NH2}$**]

One of the target optimized structures, [{(^{t}BuMeArO)$_3$tacn}Tb^{III}((*R*)-**L$_{NH2}$**)] (denoted as ^{tBu}**1$_{Tb}$**/(*R*)-**L$_{NH2}$**), was calculated. An initial structure was created by mirror inversion of the optimized structure of ^{tBu}**1$_{Tb}$**/(*S*)-**L$_{NH2}$**.

3-2. Estimation of interaction energies between ^{tBu}**1$_{Tb}$′**/^{Me}**1$_{Tb}$′** units and **L$_{NH2}$** to form ^{tBu}**1$_{Tb}$**/**L$_{NH2}$** and ^{Me}**1$_{Tb}$**/**L$_{NH2}$**

Interaction energies between {(^{R}MeArO)$_3$tacn}Tb^{III} units (denoted as ^{R}**1$_{Tb}$′**, R = *t*Bu, Me) and **L$_{NH2}$** to form ^{R}**1$_{Tb}$**/**L$_{NH2}$** were calculated as follows. A schematic is shown in **Scheme S3**. The optimized structure of ^{R}**1$_{Tb}$**/**L$_{NH2}$** was separated into parts ^{R}**1$_{Tb}$′** and **L$_{NH2}$**, and the total energies of ^{R}**1$_{Tb}$′** and **L$_{NH2}$** (denoted as E_{Tb} and E_{NH2}) were calculated by a single-point energy calculation to obtain the energy of each fragment without changing the configuration. Interaction energies, E_{int}, were calculated by

$$E_{int} = E - (E_{Tb} + E_{NH2}) \qquad (4)$$

where E is the calculated total energy of ^{R}**1$_{Tb}$**/**L$_{NH2}$**, and E_{Tb} and E_{NH2} are the single-point calculated energies of ^{R}**1$_{Tb}$′** and **L$_{NH2}$** (the fragments of ^{R}**1$_{Tb}$**/**L$_{NH2}$**), respectively.

The difference in interaction energy, ΔE_{int}, was calculated by

$$\Delta E_{int} = E_{int}(t\text{Bu}) - E_{int}(\text{Me}) \qquad (5)$$

where E_{int}(*t*Bu) and E_{int}(Me) are the calculated interaction energies of ^{tBu}**1$_{Tb}$**/**L$_{NH2}$** and ^{Me}**1$_{Tb}$**/**L$_{NH2}$**, respectively. The interaction energies were calculated based on the *Δ*- and *Λ*-configurations of the ^{tBu}**1$_{Tb}$′**/^{Me}**1$_{Tb}$′** units and on (*R*)- and (*S*)-**L$_{NH2}$** with a similar procedure. The calculated energies are listed in **Tables S6** and **S7**.

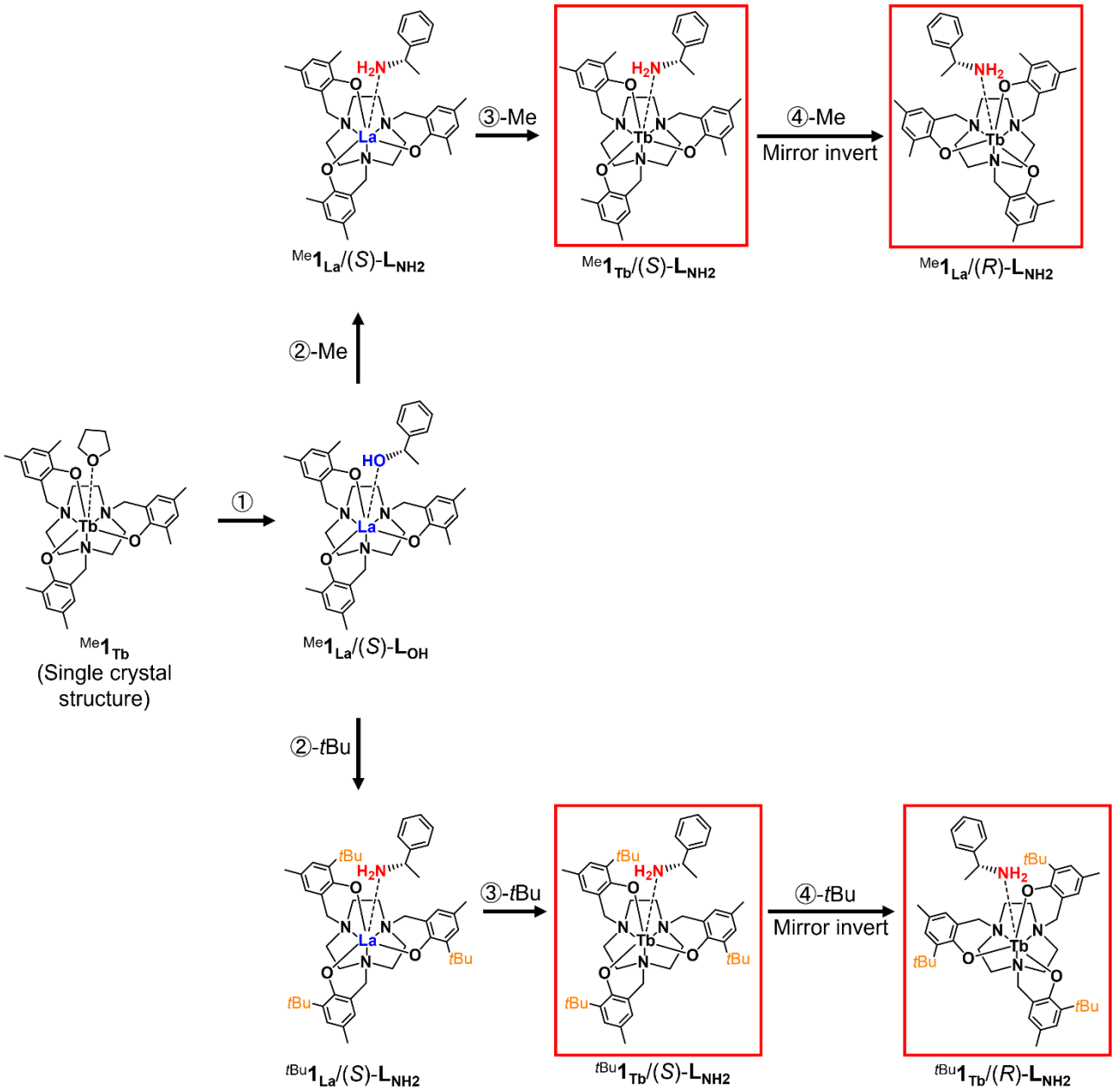

Scheme S2 Procedure for the geometry optimization of $^{Me}\mathbf{1}_{Tb}$/(*R*)- or (*S*)-$\mathbf{L}_{NH2}$ and $^{tBu}\mathbf{1}_{Tb}$/(*R*)- or (*S*)-$\mathbf{L}_{NH2}$ by DFT calculations.

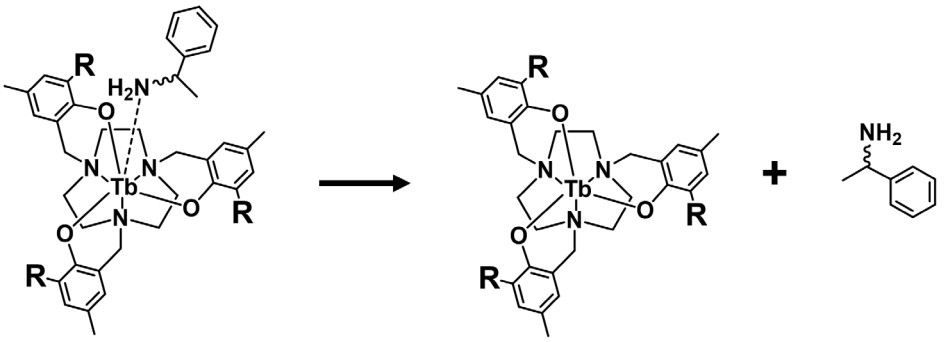

	$^{R}\mathbf{1}_{Tb}/\mathbf{L}_{NH2}$ (R = Me, *t*Bu)	$^{R}\mathbf{1}_{Tb}'$ (R = Me, *t*Bu)	$\mathbf{L}_{NH2}$
Calculation approach	Geometry optimization	Single point calculation	Single point calculation
Total energy	E	E_{Tb}	E_{NH2}
Interaction energy	$E_{int} = E - (E_{Tb} + E_{NH2})$		

Scheme S3 Procedure to estimate the interaction energies between $^{tBu}\mathbf{1}_{Tb}'/^{Me}\mathbf{1}_{Tb}'$ units and $\mathbf{L}_{NH2}$ to form $^{tBu}\mathbf{1}_{Tb}/\mathbf{L}_{NH2}$ and $^{Me}\mathbf{1}_{Tb}/\mathbf{L}_{NH2}$ based on DFT calculations.

Table S1 Crystallographic Data of $^{t\mathrm{Bu}}\mathbf{1}_{\mathbf{Tb}}$ and $^{t\mathrm{Bu}}\mathbf{1}_{\mathbf{Tb}}$/(*R*)-$\mathbf{L}_{\mathbf{NH2}}$

	$^{t\mathrm{Bu}}\mathbf{1}_{\mathbf{Tb}}$	$^{t\mathrm{Bu}}\mathbf{1}_{\mathbf{Tb}}$/(*R*)-$\mathbf{L}_{\mathbf{NH2}}$
Formula	$C_{45}H_{67}N_4O_4Tb$	$C_{50}H_{71}N_4O_3Tb{\cdot}0.5C_8H_9N$
Fw	886.98	995.66
Crystal system	$R\bar{3}$ (No. 148)	$P2_1$ (No. 4)
Space group	Trigonal	Monoclinic
a (Å)	13.9426(3)	12.5520(2)
b (Å)	13.9426(3)	36.5500(4)
c (Å)	39.4010(12)	21.8477(3)
α (deg)	90	90
β (deg)	90	100.864(10)
γ (deg)	120	90
V (Å^3)	6633.2(3)	9843.5(2)
Z	6	8
μ (mm^{-1})	1.643	1.484
F(000)	2772.0	4168.0
D_{calcd} (g/cm^3)	1.332	1.344
Temperature (K)	123	123
Reflections collected	17059	272204
Independent reflection	4086	56152
Data/parameters	4086/218	56152/2293
R_1 [$I > 2\sigma(I)$]	0.0179	0.0257
wR_2 (all data)	0.0446	0.0511
Goodness-of-fit	1.066	1.019
Flack parameter	-	0.029(4)

Table S2 Continuous Shape Measures (CSM) Values[20] Calculated for $^{t\text{Bu}}\mathbf{1}_{\mathbf{Tb}}$ and $^{t\text{Bu}}\mathbf{1}_{\mathbf{Tb}}$/(*R*)-$\mathbf{L}_{\mathbf{NH2}}$

	HP-7	HPY-7	PBPY-7	COC-7	CTPR-7	JPBPY-7	JETPY-7
$^{t\text{Bu}}\mathbf{1}_{\mathbf{Tb}}$	34.044	20.914	9.527	1.199	3.031	12.379	12.793
$^{t\text{Bu}}\mathbf{1}_{\mathbf{Tb}}$/(*R*)-$\mathbf{L}_{\mathbf{NH2}}$	32.877	20.154	7.881	1.885	3.056	10.398	12.236

HP-7 (D_{7h}) Heptagon
HPY-7 (C_{6v}) Hexagonal pyramid
PBPY-7 (D_{5h}) Pentagonal bipyramid
COC-7 (C_{3v}) Monocapped octahedron (capped octahedron)
CTPR-7 (C_{2v}) Monocapped trigonal prism (capped trigonal prism)
JPBPY-7 (D_{5h}) Johnson pentagonal bipyramid (J13)
JETPY-7 (C_{3v}) Johnson elongated triangular pyramid (J7)

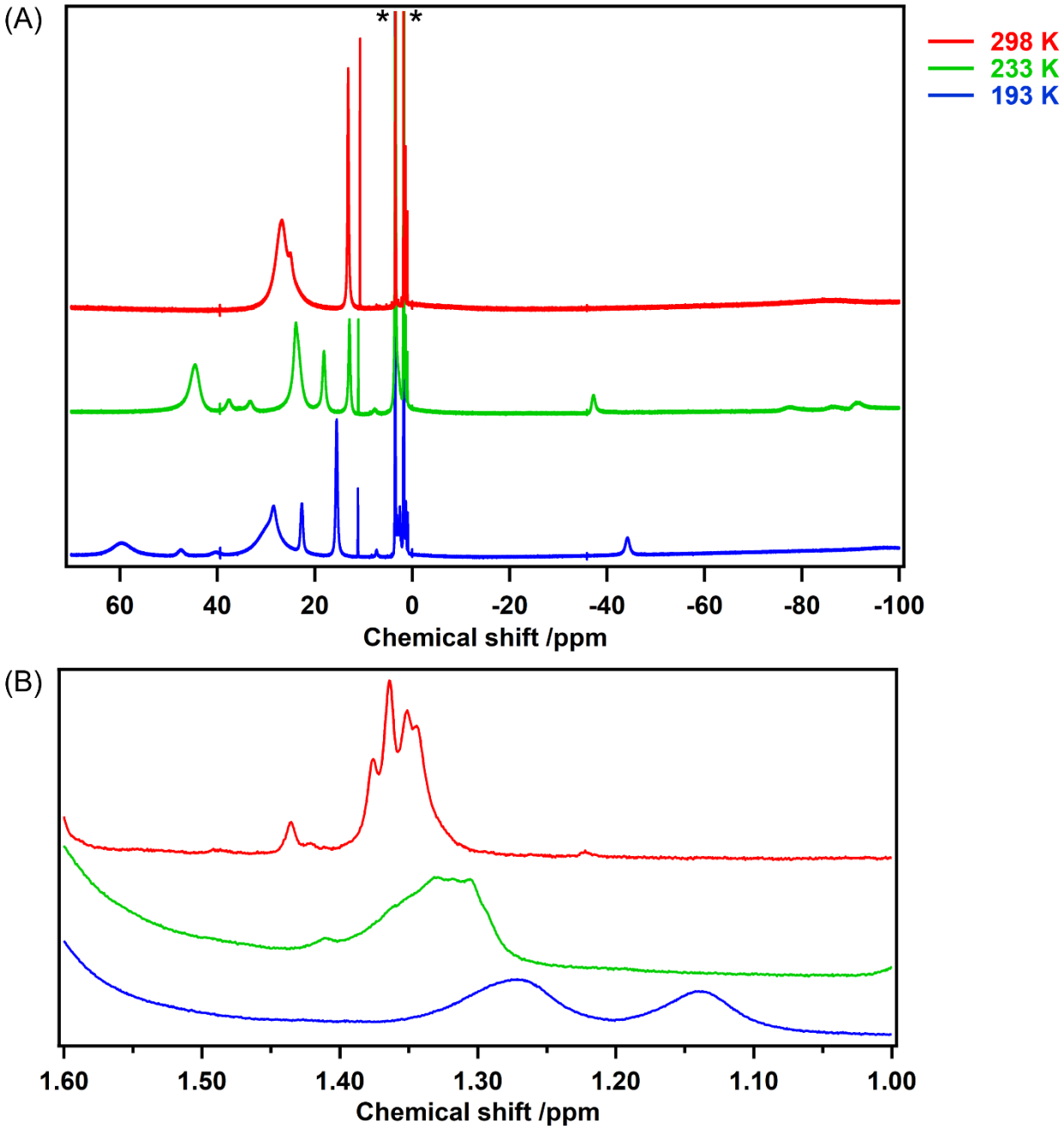

Fig. S1 VT ^{1}H NMR (14.0 T, 600 MHz, THF-d_8) of $^{t\mathrm{Bu}}\mathbf{1}_{\mathbf{Tb}}$ at 298, 233, and 193 K. (A) Whole range (70 – −100 ppm). Peaks denoted as * are residual signals of THF. (B) In the range of 1.60 – 1.00 ppm. Peak at 1.38 – 1.34 ppm at 298 K could be attributed to the protons of the *t*Bu groups, and the peak was split by cooling down from 233 K to 193 K. (C) In the range of 65 – 10 ppm. (D) In the range of 4.0 – 0.5 ppm. (E) In the range of −30 – −100 ppm.

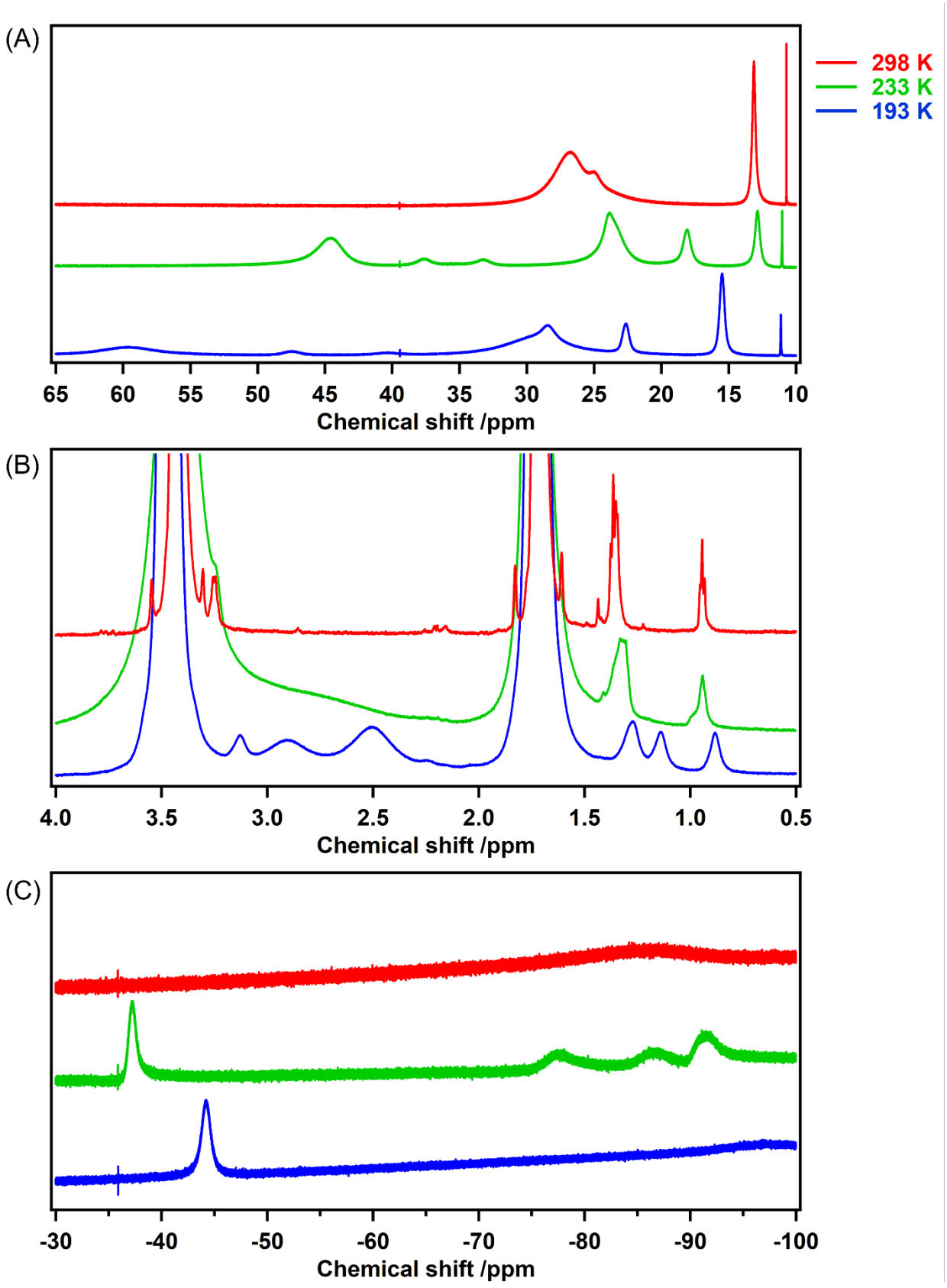

Fig. S1 (Continued) VT ^{1}H NMR (14.0 T, 600 MHz, THF-d_8) of $^{t\mathrm{Bu}}\mathbf{1}_{\mathbf{Tb}}$ at 298, 233, and 193 K. (A) Whole range (70 – −100 ppm). Peaks denoted as * are residual signals of THF. (B) In the range of 1.60 – 1.00 ppm. Peak at 1.38 – 1.34 ppm at 298 K could be attributed to the protons of the *t*Bu groups, and the peak was split by cooling down from 233 K to 193 K. (C) In the range of 65 – 10 ppm. (D) In the range of 4.0 – 0.5 ppm. (E) In the range of −30 – −100 ppm.

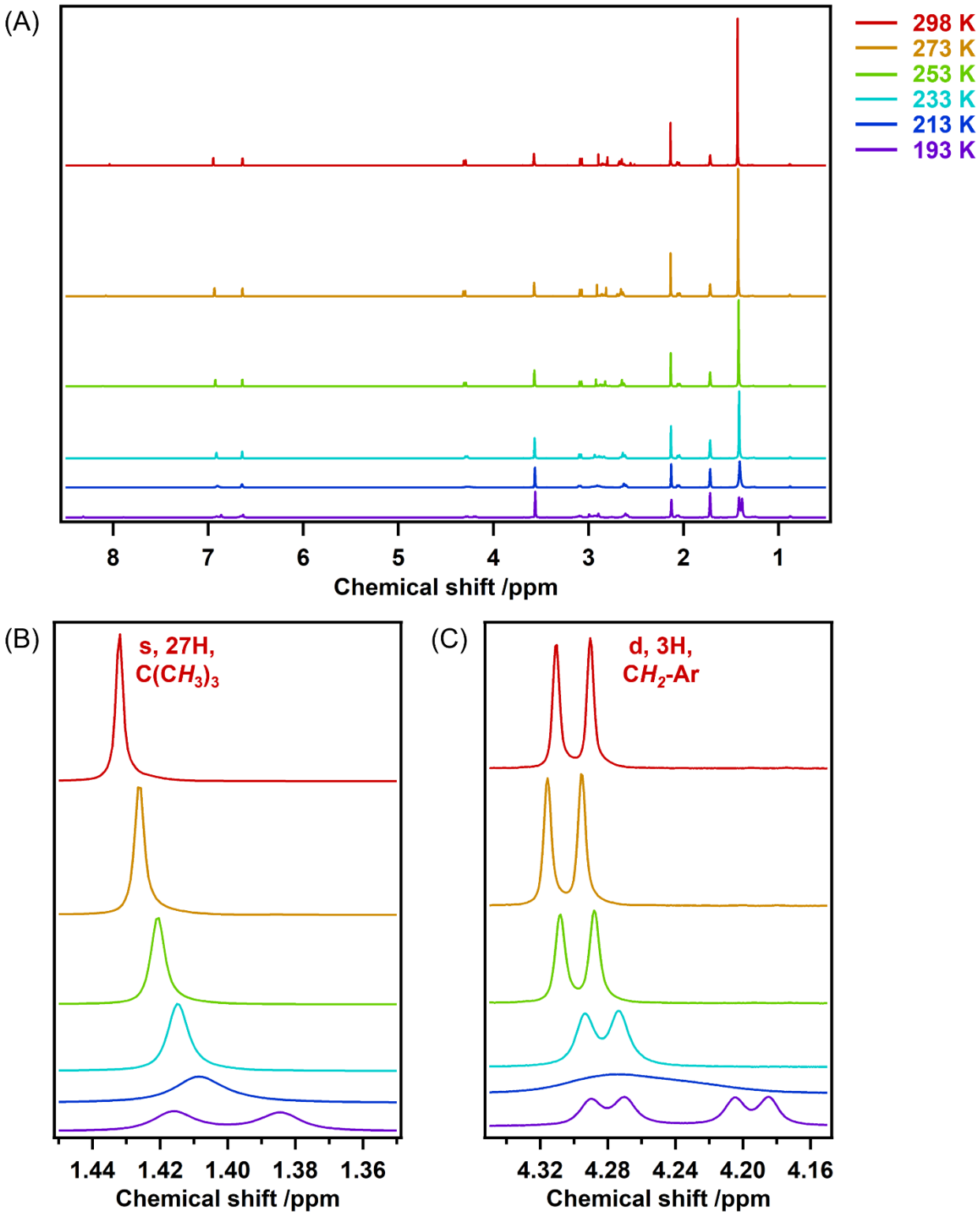

Fig. S2 VT ^{1}H NMR (14.0 T, 600 MHz, THF-d_8) of $^{t\mathrm{Bu}}$**1**$_{\mathrm{Y}}$ at 298, 273, 253, 233, 213, and 193 K. (A) Whole range (8.5 – 0.5 ppm). (B) In the range of 1.45 – 1.35 ppm. (C) In the range of 4.35 – 4.15 ppm. (D) In the range of 8.50 – 6.00 ppm. (E) In the range of 3.20 – 2.78 ppm. (F) In the range of 2.79 – 1.90 ppm.

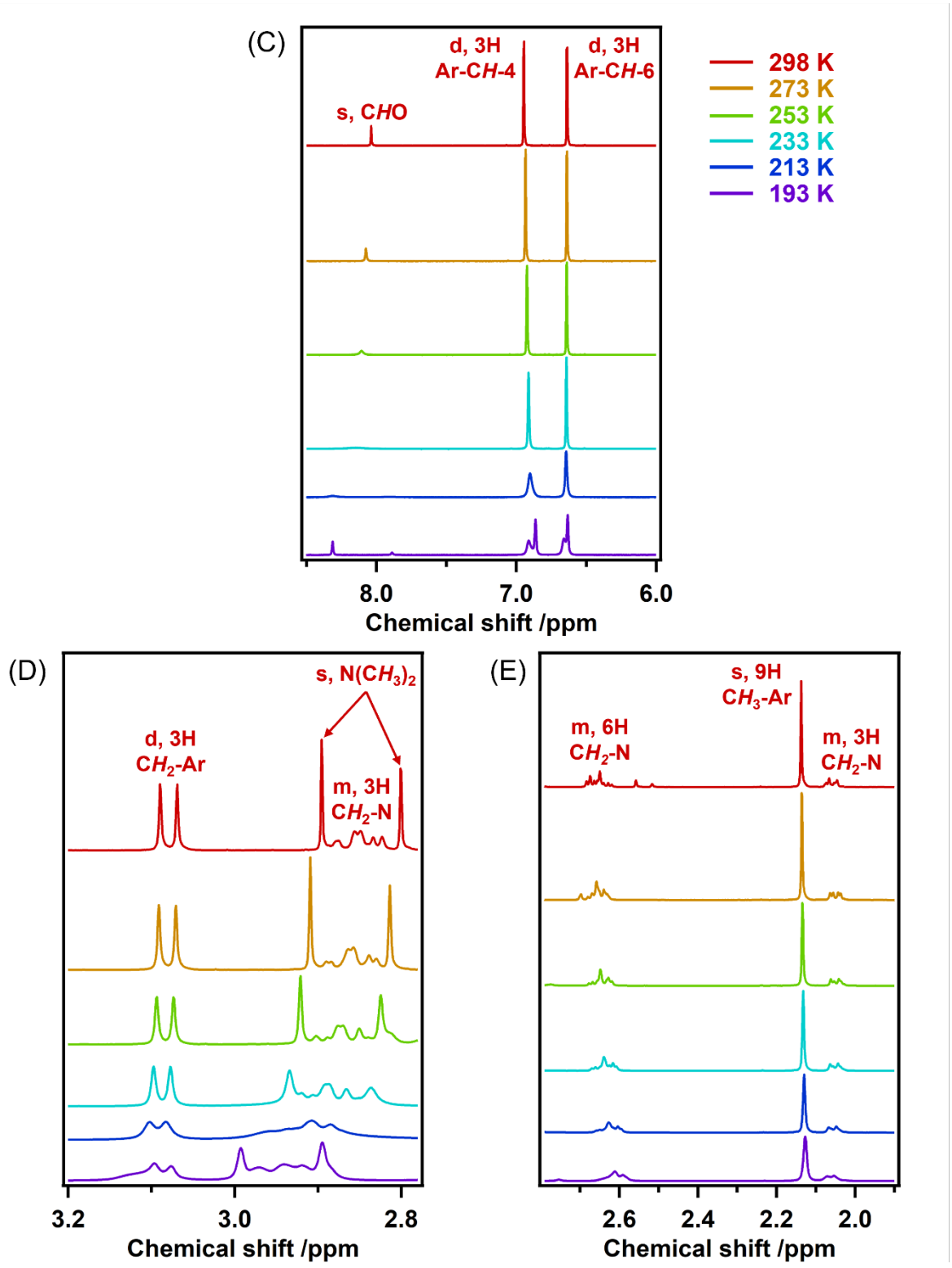

Fig. S2 (Continued) VT ^{1}H NMR (14.0 T, 600 MHz, THF-d_8) of $^{t\mathrm{Bu}}\mathbf{1}_{\mathrm{Y}}$ at 298, 273, 253, 233, 213, and 193 K. (A) Whole range (8.5 – 0.5 ppm). (B) In the range of 1.45 – 1.35 ppm. (C) In the range of 4.35 – 4.15 ppm. (D) In the range of 8.50 – 6.00 ppm. (E) In the range of 3.20 – 2.78 ppm. (F) In the range of 2.79 – 1.90 ppm.

Table S3 Observation of ^{1}H NMR Peak Changes in the VT ^{1}H NMR Experiment of $^{t\mathrm{Bu}}\mathbf{1}_{\mathbf{Y}}$

Chemical shift of peak (ppm) at 298 K	Attribution	Observation during VT ^{1}H NMR experiment
1.43 (s, 27H; C(C*H*$_3$)$_3$)	*t*Bu groups at the *ortho*-position of the phenoxide moieties	This peak was observed as one singlet peak above 213 K. **It was split to two peaks at 193 K (Fig. S2(B))**. Peak was shifted to high field when decreasing temperature.
2.14 (s, 9H; C*H*$_3$-Ar)	Methyl groups at the *para*-position of the phenoxide moieties	This peak was observed as one singlet peak in the range of 298 K – 193 K (**Fig. S2(F)**). Peak was slightly shifted to high field and when decreasing temperature.
2.07−2.03, 2.88−2.82 (m, 3H; C*H*$_2$-N)	Methylene groups of tacn ligand	These peaks were observed as multiplet peaks in the range of 298 K – 193 K (**Fig. S2(E, F)**). Peaks were slightly shifted to low field when decreasing temperature.
2.68−2.62 (m, 6H; C*H*$_2$-N)	Methylene groups of tacn ligand	These peaks were observed as multiplet peaks in the range of 298 K – 193 K (**Fig. S2(F)**). Peaks were slightly shifted to high field when decreasing temperature.
2.80, 2.90 (s; N(C*H*$_3$)$_2$)	Methyl groups of DMF	These peaks were observed as one singlet peak above 233 K. **They were observed to be disappeared at 213 K and reappeared at 193 K** (**Fig. S2(E)**). Peaks were shifted to low field when decreasing temperature.
3.08 (d, *J* = 12.4 Hz, 3H; C*H*$_2$-Ar)	Methylene groups between tacn and phenoxide moieties	This peak was observed as one doublet peak in the range of 298 K – 193 K (**Fig. S2(E)**). Peak was slightly shifted to low field when decreasing temperature.
4.30 (d, *J* = 11.9 Hz, 3H; C*H*$_2$-Ar)	Methylene groups between tacn and phenoxide moieties	This peak was observed as one doublet peak above 233 K. **They were observed to be one broad peak at 213 K and reappeared at 193 K with two doublet peaks** (**Fig. S2(C)**). Peak was shifted to high field when decreasing temperature.
6.64 (d, *J* = 2.3 Hz, 3H; Ar-C*H*-6)	Aromatic groups of phenoxide moieties	This peak was observed as one doublet peak above 253 K. **It was observed to be one broad peak at 233 K and 213 K and was split into two peaks at 193 K** (**Fig. S2(D)**). Peak position was almost steady when decreasing temperature.
6.95 (d, *J* = 2.3 Hz, 3H; Ar-C*H*-4)	Aromatic groups of phenoxide moieties	This peak was observed as one doublet peak above 253 K. **It was observed to be one broad peak at 233 K and 213 K and was split into two peaks at 193 K** (**Fig. S2(D)**). Peak was shifted to high field when decreasing temperature.
8.04 (s; C*H*O)	Aldehyde group of DMF	This peak was observed as one singlet peak above 253 K. **It was observed to be one broad peak at 233 K, and was split into two broad peaks (8.31 and 7.90 ppm) at 213 K. They were observed to be two sharp singlet peaks at 193 K** (**Fig. S2(D)**). Peak was shifted to low field when decreasing temperature.

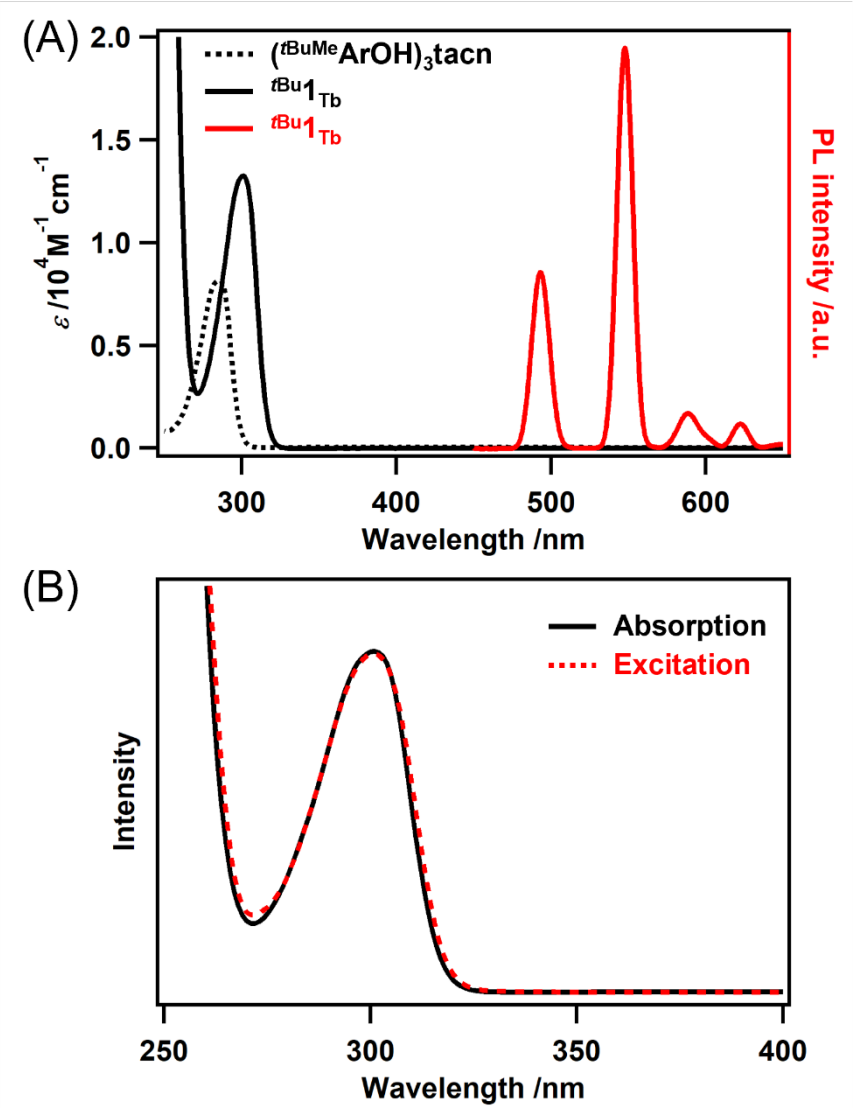

Fig. S3 (A) UV-vis absorption spectra of ($^{t\text{BuMe}}$ArOH)$_3$tacn and $^{t\text{Bu}}$**1**$_{\text{Tb}}$, and total luminescence spectra of $^{t\text{Bu}}$**1**$_{\text{Tb}}$ (λ_{ex} = 300 nm) in THF at 293 K (UV-vis: [($^{t\text{BuMe}}$ArOH)$_3$tacn] = 1.2×10^{-4} mol L^{-1}, [$^{t\text{Bu}}$**1**$_{\text{Tb}}$] = 7.6×10^{-5} mol L^{-1}; PL: [$^{t\text{Bu}}$**1**$_{\text{Tb}}$] = 2.7×10^{-6} mol L^{-1}). (B) UV-vis absorption and excitation (λ_{em} = 547 nm) spectra of $^{t\text{Bu}}$**1**$_{\text{Tb}}$ in THF at 293 K (UV-vis: [$^{t\text{Bu}}$**1**$_{\text{Tb}}$] = 7.6×10^{-5} mol L^{-1}; excitation: [$^{t\text{Bu}}$**1**$_{\text{Tb}}$] = 2.7×10^{-6} mol L^{-1}).

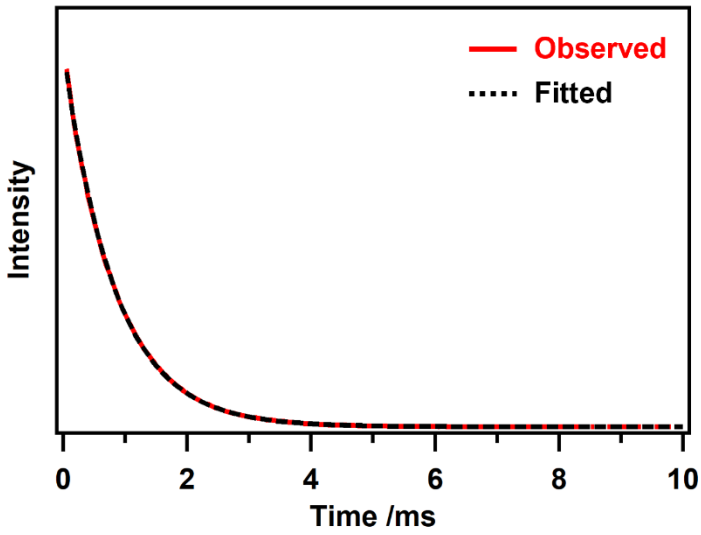

Fig. S4 Luminescence decay curve of $^{t\mathrm{Bu}}\mathbf{1}_{\mathbf{Tb}}$ under Ar (solid red line, 820 μs) in THF at 293 K. The decay was monitored at 547 nm (λ_{ex} = 300 nm). The observed curve was fitted by a single exponential function (dotted black line).

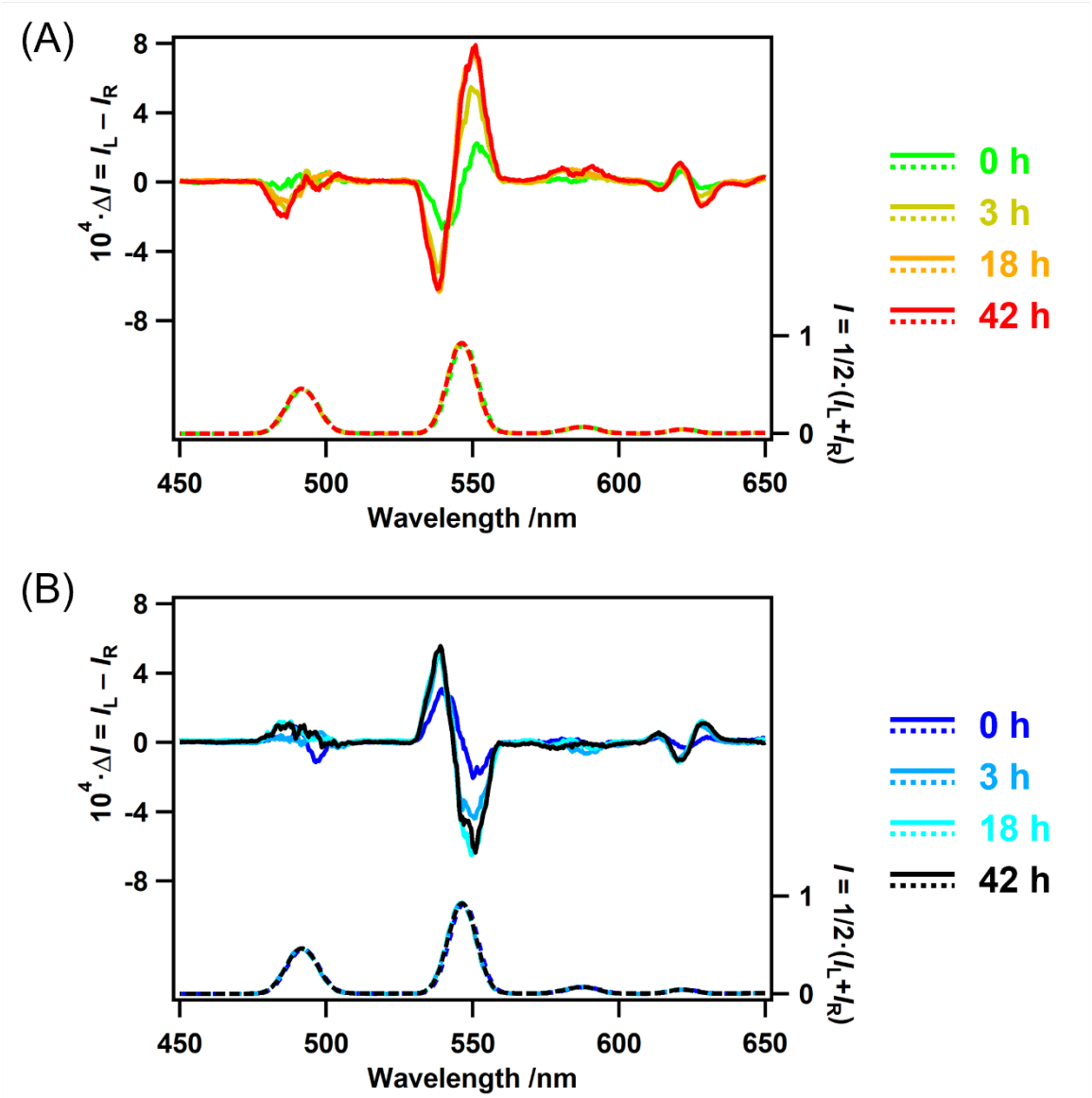

Fig. S5 CPL (solid line) and total luminescence (dotted line) spectra of $^{t\mathrm{Bu}}\mathbf{1}_{\mathbf{Tb}}$ 0, 3, 18, and 42 h after adding 3000 equivalents of (A) (*S*)-$\mathbf{L}_{\mathbf{NH2}}$ or (B) (*R*)-$\mathbf{L}_{\mathbf{NH2}}$ in THF at 293 K. [$^{t\mathrm{Bu}}\mathbf{1}_{\mathbf{Tb}}$] = 1×10^{-3} mol L^{-1}.

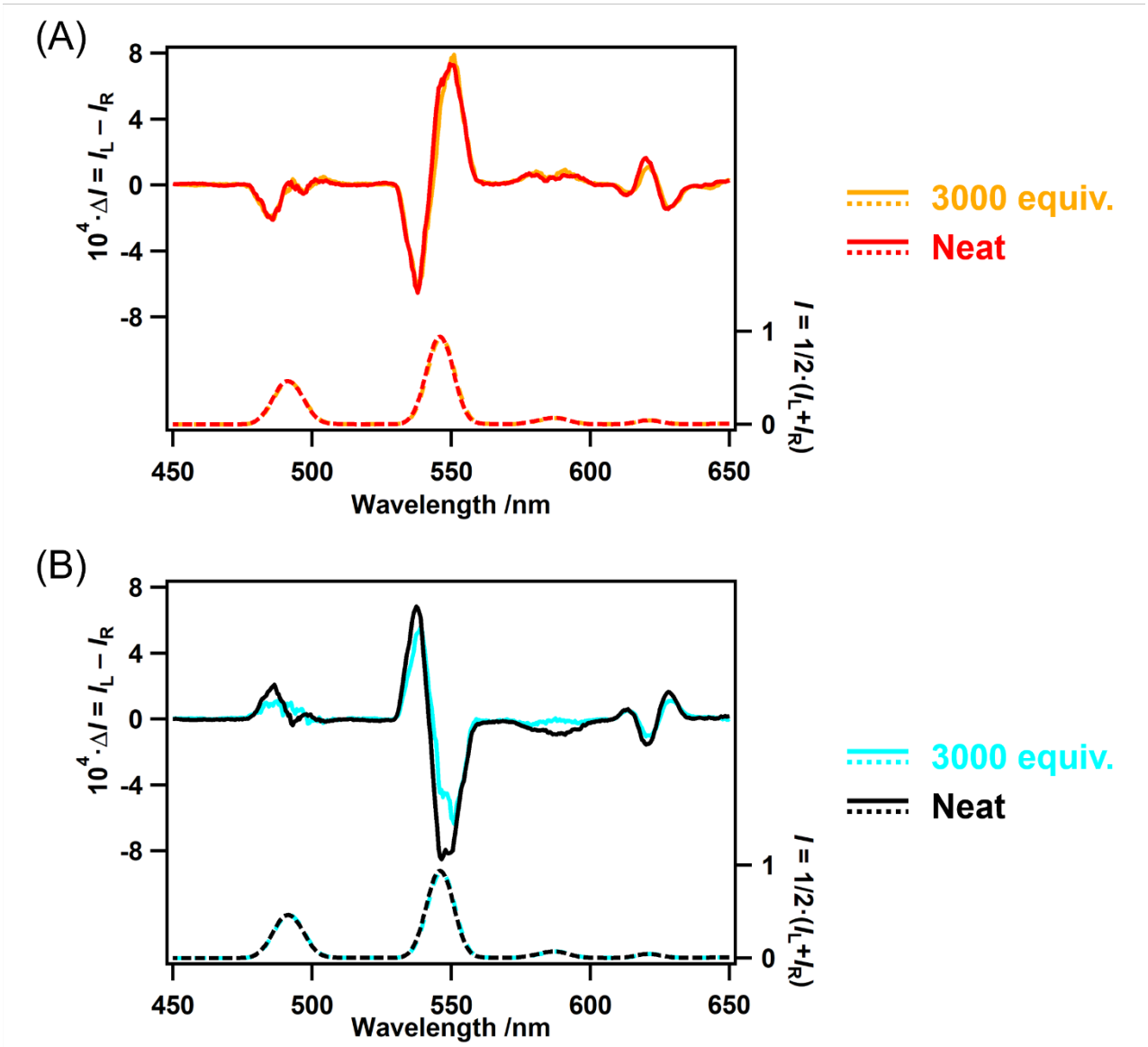

Fig. S6 CPL (solid line) and total luminescence (dotted line) spectra of $^{t\mathrm{Bu}}\mathbf{1}_{\mathbf{Tb}}$ with (A) (*S*)-$\mathbf{L}_{\mathbf{NH2}}$ and (B) (*R*)-$\mathbf{L}_{\mathbf{NH2}}$ at 293 K. 3000 equiv.: 3000 equivalents of $\mathbf{L}_{\mathbf{NH2}}$ was added to the THF solution of $^{t\mathrm{Bu}}\mathbf{1}_{\mathbf{Tb}}$ ($[^{t\mathrm{Bu}}\mathbf{1}_{\mathbf{Tb}}] = 1 \times 10^{-3}$ mol L^{-1}). Neat: $^{t\mathrm{Bu}}\mathbf{1}_{\mathbf{Tb}}$ was added to $\mathbf{L}_{\mathbf{NH2}}$ ($[^{t\mathrm{Bu}}\mathbf{1}_{\mathbf{Tb}}] = 4 \times 10^{-3}$ mol L^{-1}). All spectra were measured more than 18 h after adding (*S*)- or (*R*)-$\mathbf{L}_{\mathbf{NH2}}$.

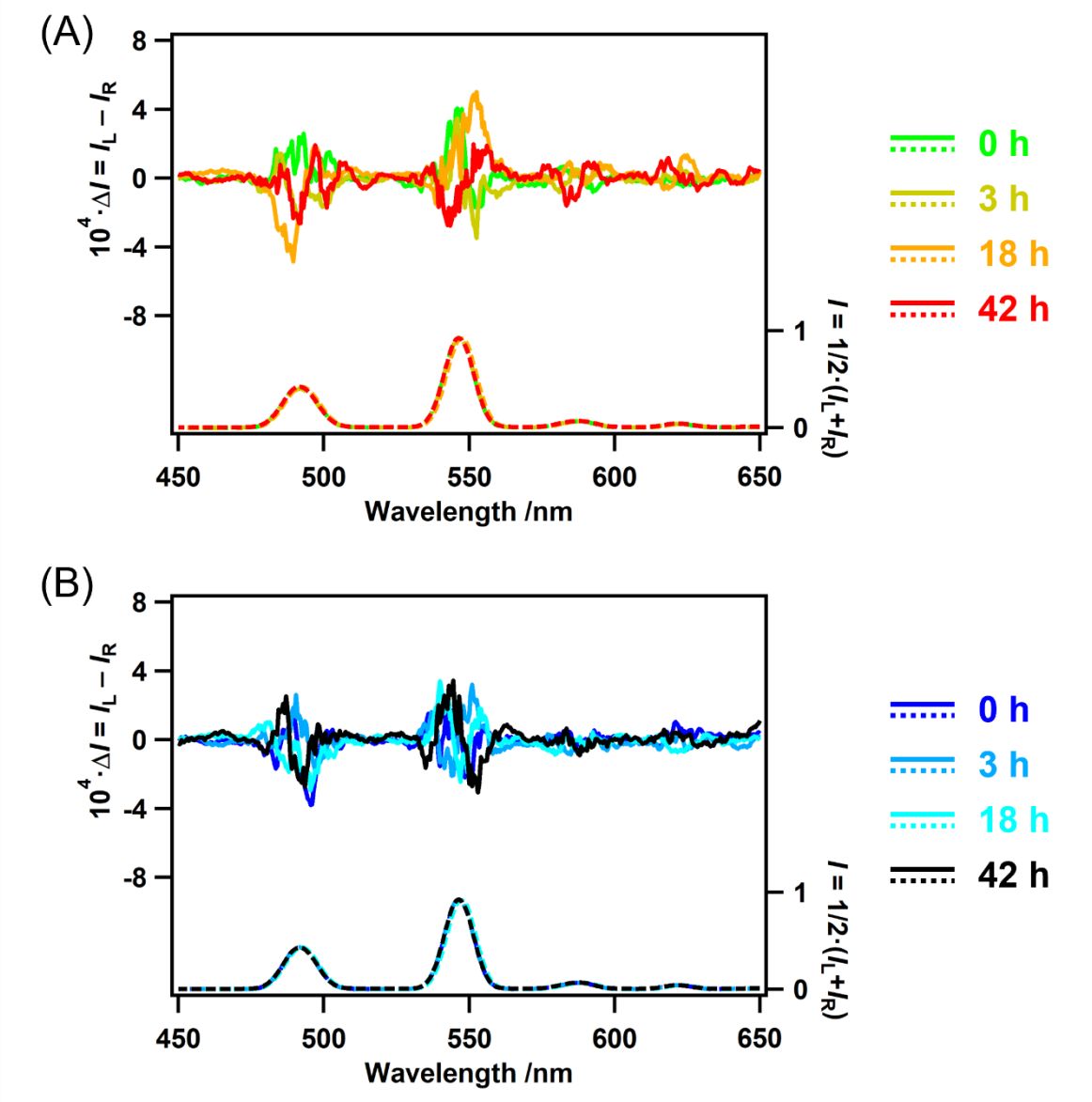

Fig. S7 CPL (solid line) and total luminescence (dotted line) spectra of $^{t\mathrm{Bu}}\mathbf{1}_{\mathrm{Tb}}$ 0, 3, 18, and 42 h after adding 3000 equivalents of (A) (*S*)-**L**$_{\mathrm{OH}}$ or (B) (*R*)-**L**$_{\mathrm{OH}}$ in THF at 293 K. [$^{t\mathrm{Bu}}\mathbf{1}_{\mathrm{Tb}}$] = 1×10^{-3} mol L^{-1}.

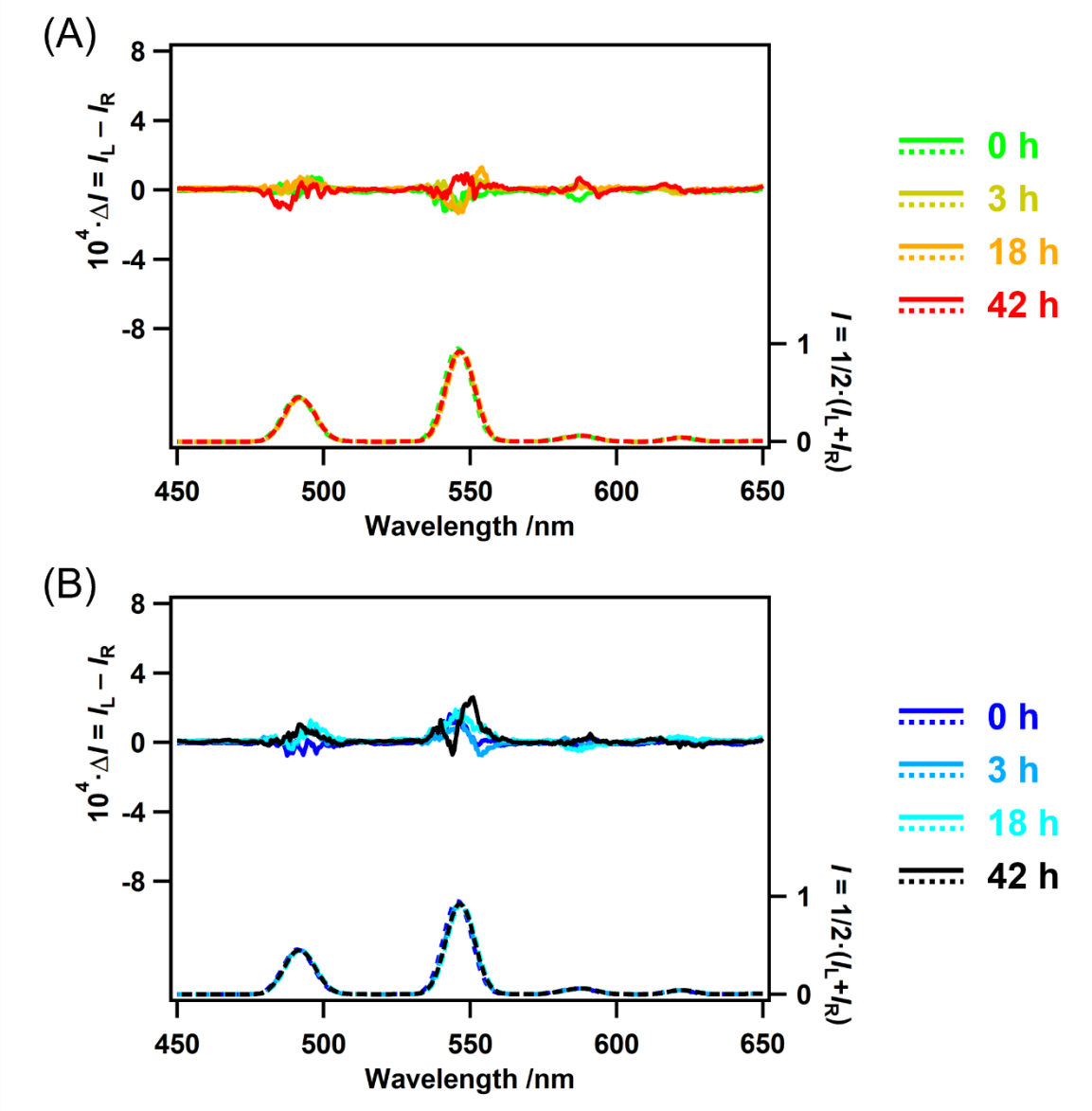

Fig. S8 CPL (solid line) and total luminescence (dotted line) spectra of $^{t\mathrm{Bu}}\mathbf{1}_{\mathbf{Tb}}$ 0, 3, 18, and 42 h after adding 1000 equivalents of (A) (*S*)-$\mathbf{L}_{\mathbf{NHAc}}$ or (B) (*R*)-$\mathbf{L}_{\mathbf{NHAc}}$ in THF at 293 K. [$^{t\mathrm{Bu}}\mathbf{1}_{\mathbf{Tb}}$] = 1×10^{-3} mol L^{-1}.

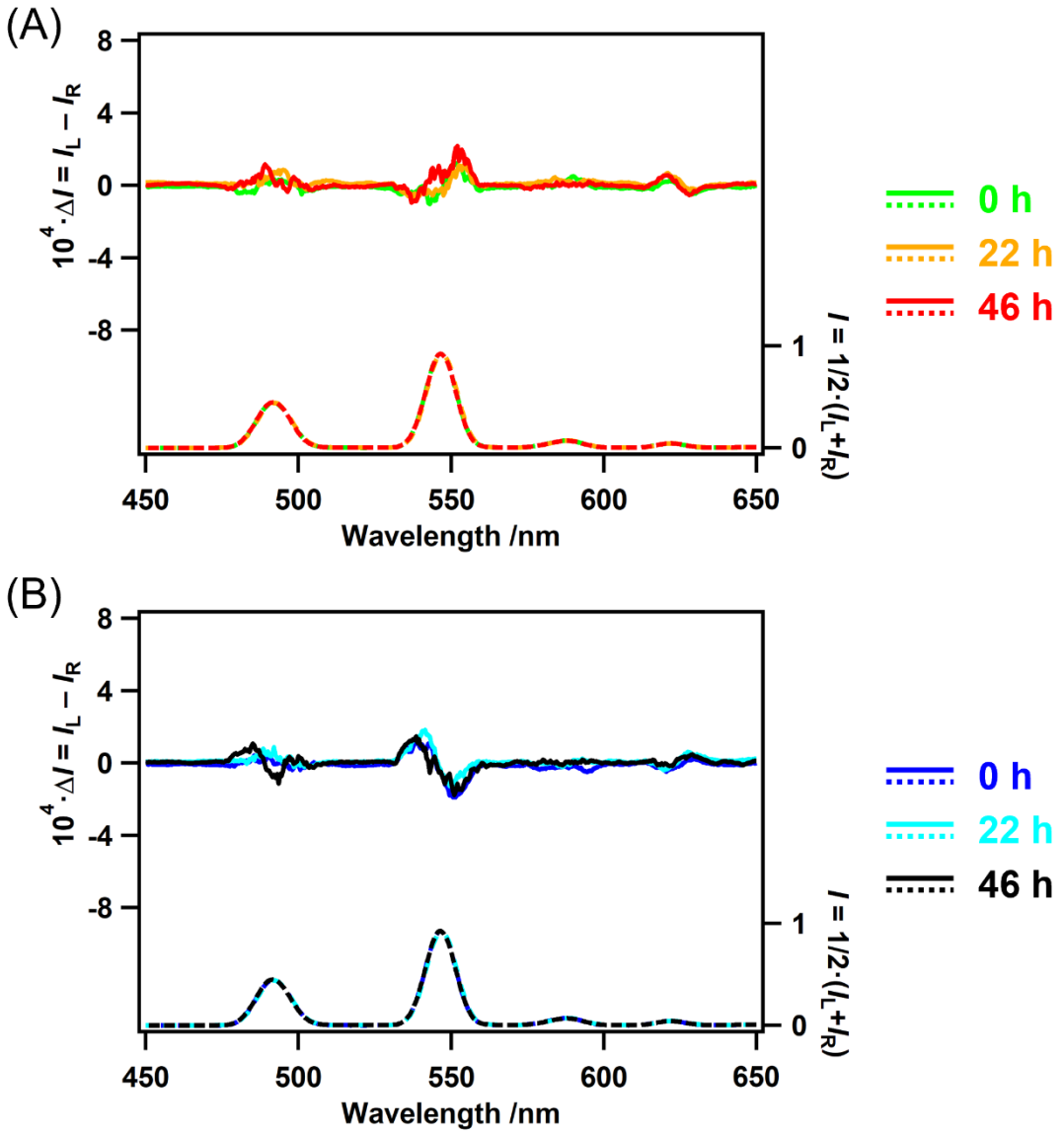

Fig. S9 CPL (solid line) and total luminescence (dotted line) spectra of $^{Me}\mathbf{1}_{Tb}$ 0, 22, and 46 h after adding 3000 equivalents of (A) (*S*)-$\mathbf{L}_{NH2}$ or (B) (*R*)-$\mathbf{L}_{NH2}$ in THF at 293 K. [$^{Me}\mathbf{1}_{Tb}$] = 1×10^{-3} mol L^{-1}.

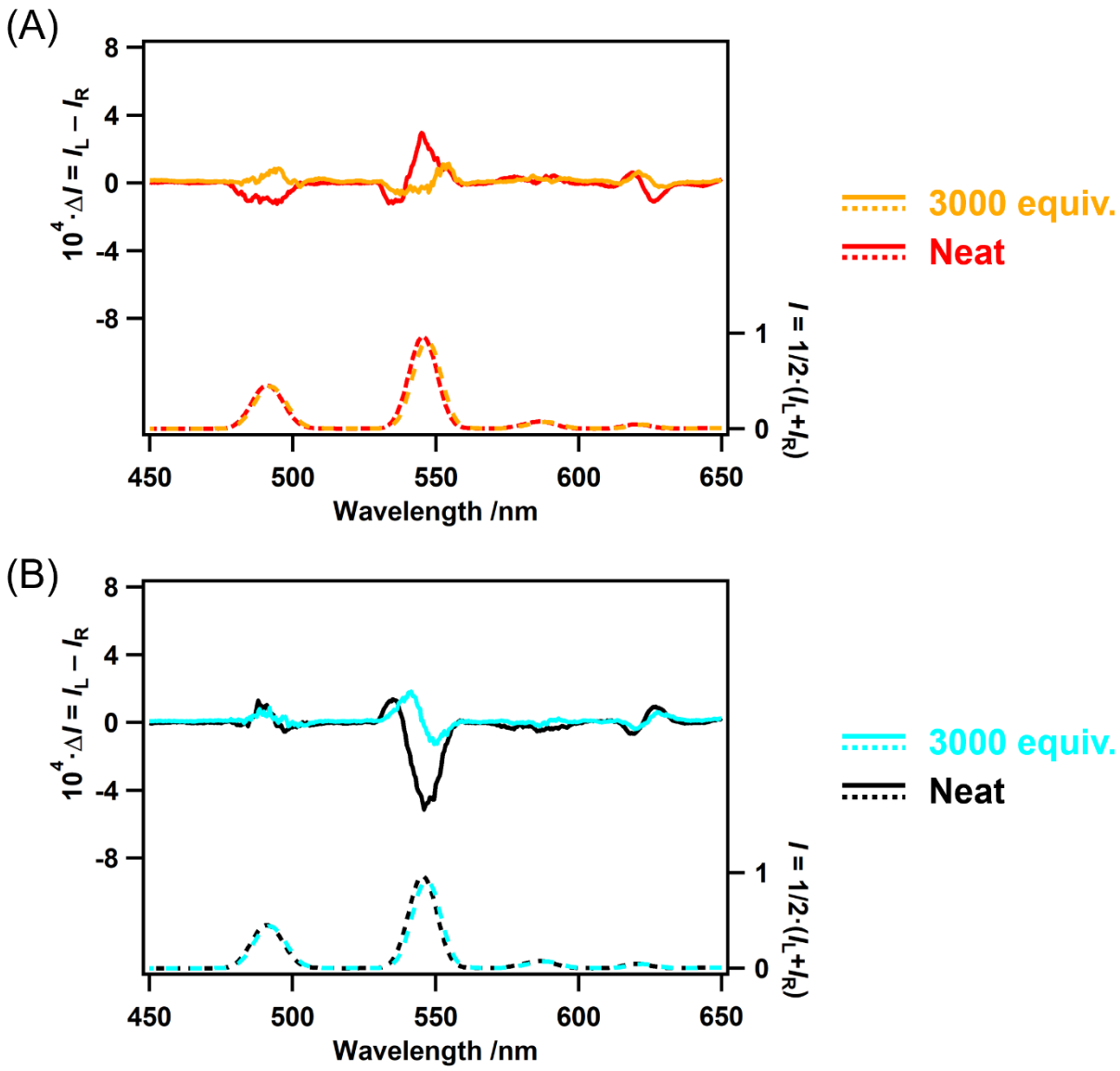

Fig. S10 CPL (solid line) and total luminescence (dotted line) spectra of $^{Me}\mathbf{1}_{Tb}$ with (A) (*S*)-$\mathbf{L}_{NH2}$ and (B) (*R*)-$\mathbf{L}_{NH2}$ at 293 K. 3000 equiv.: 3000 equivalents of $\mathbf{L}_{NH2}$ was added to the THF solution of $^{Me}\mathbf{1}_{Tb}$ ($[^{Me}\mathbf{1}_{Tb}] = 1 \times 10^{-3}$ mol L^{-1}). Neat: $^{Me}\mathbf{1}_{Tb}$ was added to $\mathbf{L}_{NH2}$ ($[^{Me}\mathbf{1}_{Tb}] = 4 \times 10^{-3}$ mol L^{-1}). All spectra were measured more than 18 h after adding (*S*)- or (*R*)-$\mathbf{L}_{NH2}$.

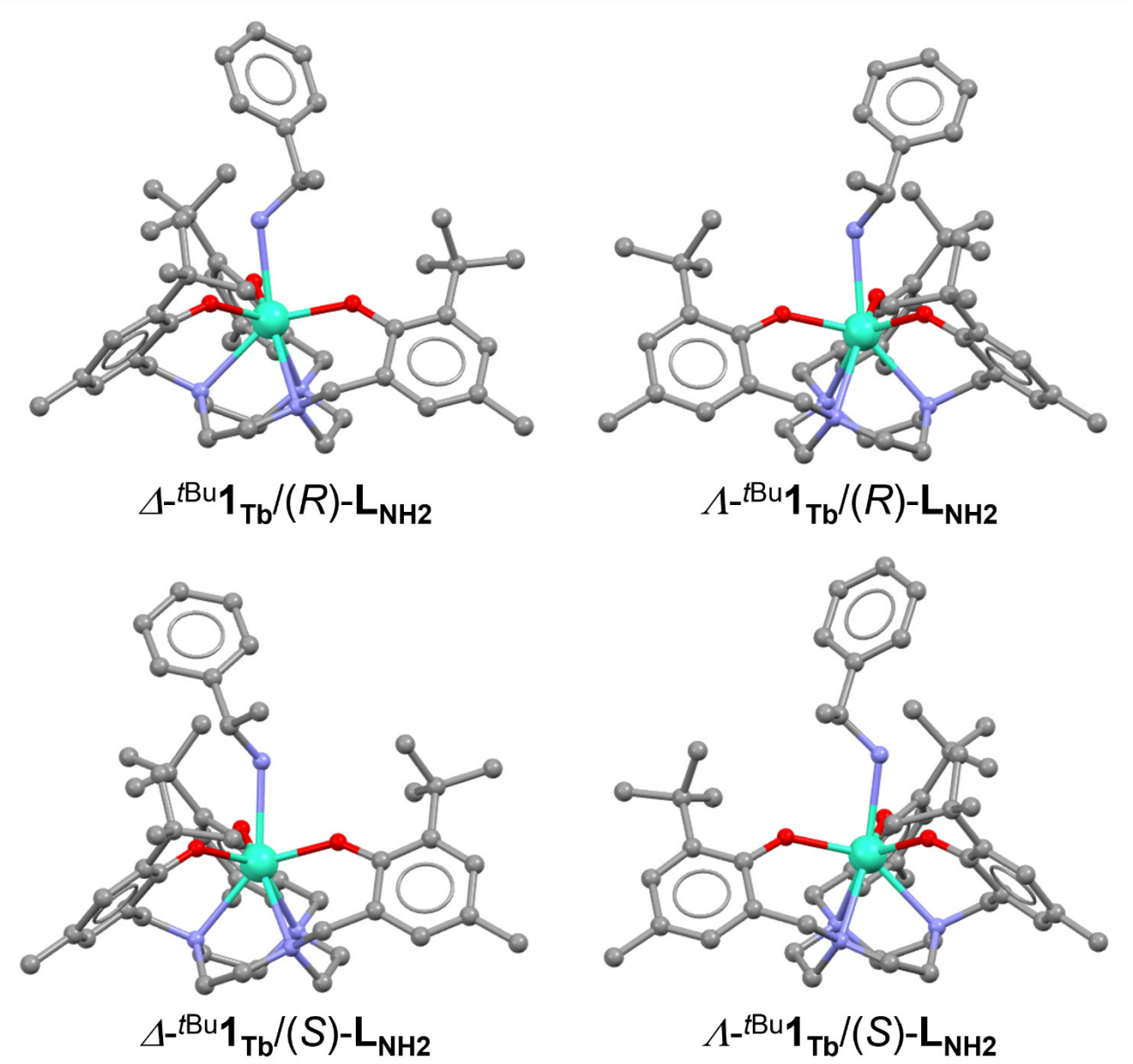

Fig. S11 Optimized structures of $^{t\mathrm{Bu}}\mathbf{1}_{\mathrm{Tb}}/\mathbf{L}_{\mathrm{NH2}}$ at the DFT/B3LYP-D3BJ level (ECP54MWB (Tb)/6-31G(d) (C, H, N, O), in THF (SAS)). H atoms are omitted for clarity. C: gray; N: blue; O: red; Tb: emerald green.

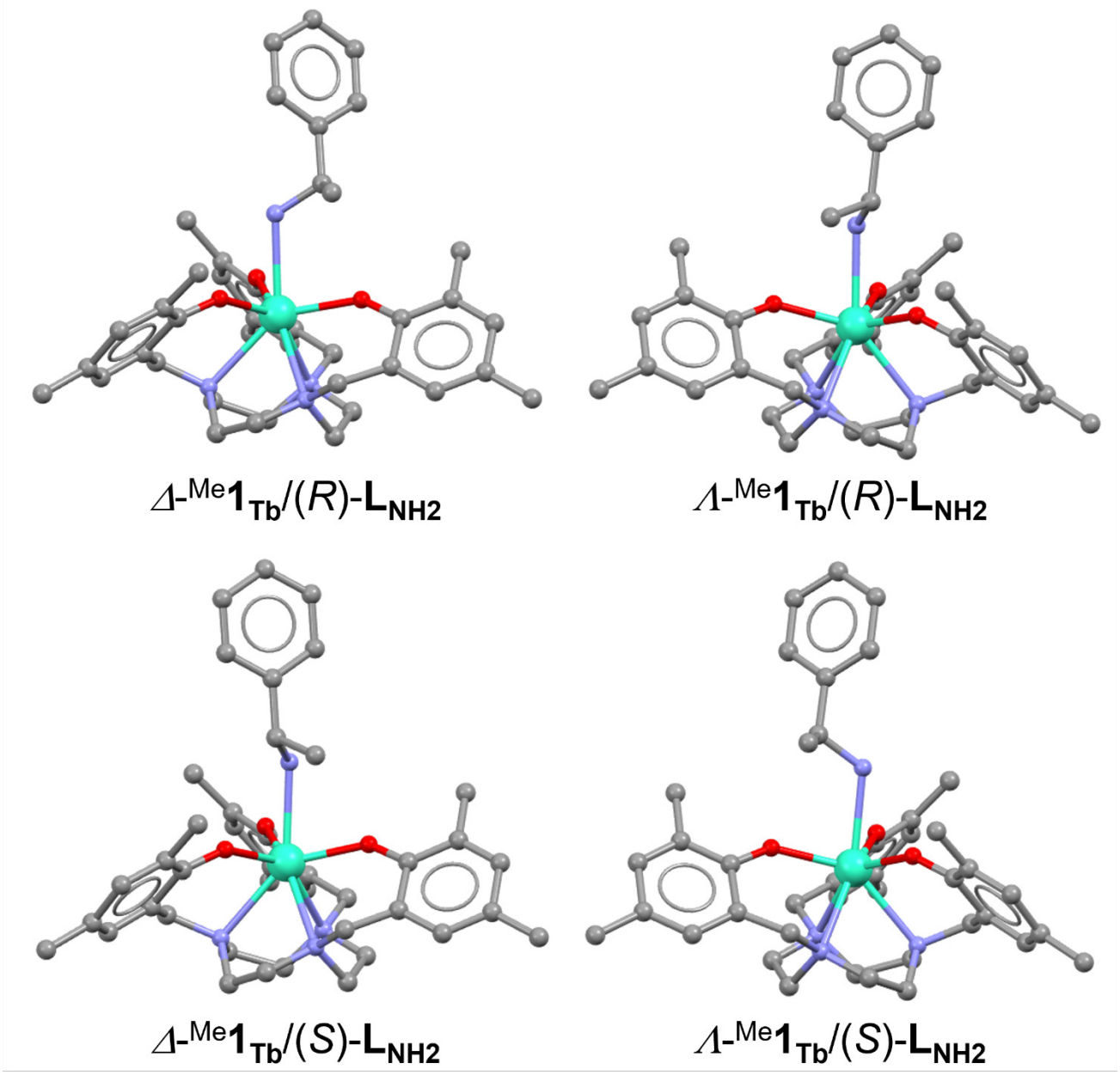

Fig. S12 Optimized structures of $^{Me}\mathbf{1}_{Tb}/\mathbf{L}_{NH2}$ at the DFT/B3LYP-D3BJ level (ECP54MWB (Tb)/6-31G(d) (C, H, N, O), in THF (SAS)). H atoms are omitted for clarity. C: gray; N: blue; O: red; Tb: emerald green.

Table S4 Total Energy (E) and Energy Difference (ΔE) of $^{t\mathrm{Bu}}\mathbf{1}_{\mathbf{Tb}}$/($R$)- or ($S$)-$\mathbf{L}_{\mathbf{NH2}}$ (Δ- and Λ-isomers) Calculated at the DFT/B3LYP-D3BJ Level (ECP54MWB (Tb)/6-31G(d) (C, H, N, O), in THF (SAS))

	E /kcal mol^{-1}	ΔE /kcal mol^{-1}
Δ-$^{t\mathrm{Bu}}\mathbf{1}_{\mathbf{Tb}}$/($R$)-$\mathbf{L}_{\mathbf{NH2}}$	−1,524,550.84	-
Λ-$^{t\mathrm{Bu}}\mathbf{1}_{\mathbf{Tb}}$/($R$)-$\mathbf{L}_{\mathbf{NH2}}$	−1,524,550.68	+0.15
Δ-$^{t\mathrm{Bu}}\mathbf{1}_{\mathbf{Tb}}$/($S$)-$\mathbf{L}_{\mathbf{NH2}}$	−1,524,550.69	+0.14
Λ-$^{t\mathrm{Bu}}\mathbf{1}_{\mathbf{Tb}}$/($S$)-$\mathbf{L}_{\mathbf{NH2}}$	−1,524,550.89	−0.05

Table S5 Total Energy (E) and Energy Difference (ΔE) of $^{\mathrm{Me}}\mathbf{1}_{\mathbf{Tb}}$/($R$)- or ($S$)-$\mathbf{L}_{\mathbf{NH2}}$ (Δ- and Λ-isomers) Calculated at the DFT/B3LYP-D3BJ Level (ECP54MWB (Tb)/6-31G(d) (C, H, N, O), in THF (SAS))

	E /kcal mol^{-1}	ΔE /kcal mol^{-1}
Δ-$^{\mathrm{Me}}\mathbf{1}_{\mathbf{Tb}}$/($R$)-$\mathbf{L}_{\mathbf{NH2}}$	−1,302,497.32	-
Λ-$^{\mathrm{Me}}\mathbf{1}_{\mathbf{Tb}}$/($R$)-$\mathbf{L}_{\mathbf{NH2}}$	−1,302,497.64	−0.32
Δ-$^{\mathrm{Me}}\mathbf{1}_{\mathbf{Tb}}$/($S$)-$\mathbf{L}_{\mathbf{NH2}}$	−1,302,497.65	−0.33
Λ-$^{\mathrm{Me}}\mathbf{1}_{\mathbf{Tb}}$/($S$)-$\mathbf{L}_{\mathbf{NH2}}$	−1,302,497.32	+0.00

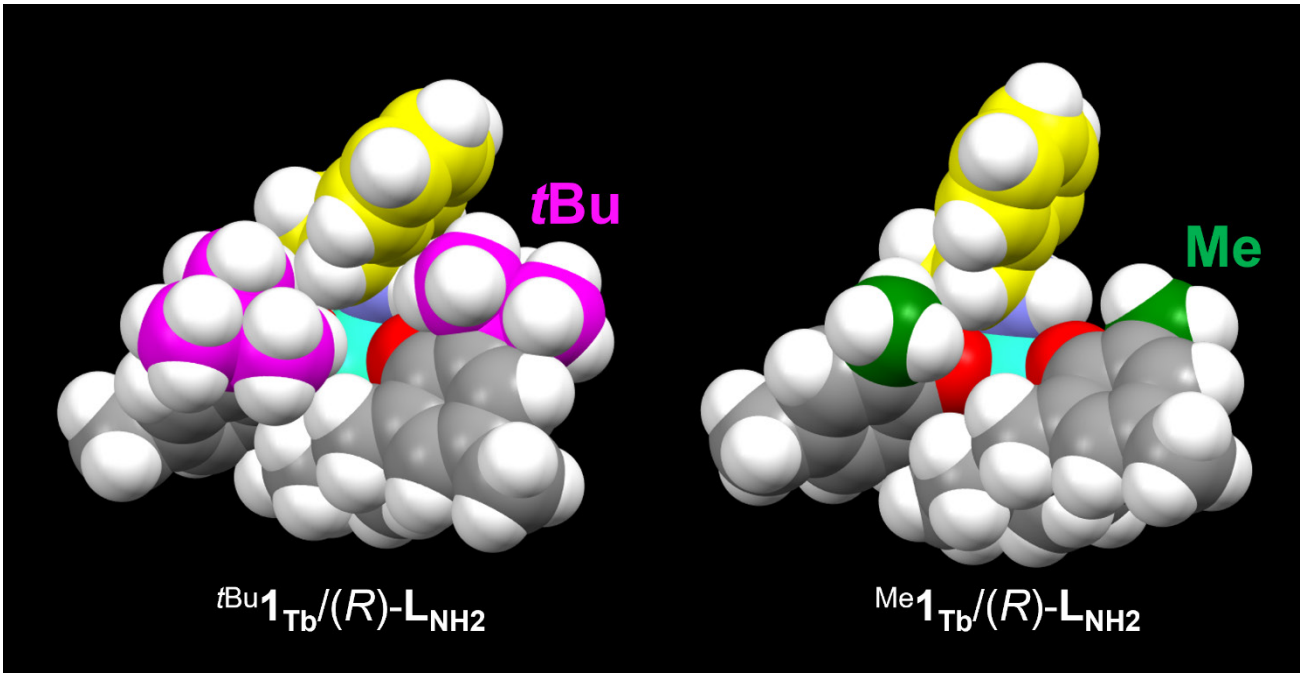

Fig. S13 Space-filling models of the calculated structures of $^{R}\mathbf{1}_{\mathbf{Tb}}$/(*R*)-$\mathbf{L}_{\mathbf{NH2}}$ (*Δ*-isomers, R = *t*Bu, Me) at the DFT/B3LYP-D3BJ level (ECP54MWB (Tb)/6-31G(d) (C, H, N, O), in THF (SAS)). H: white; *t*Bu group C: magenta; Me group C: dark green; $\mathbf{L}_{\mathbf{NH2}}$ C: yellow; other C: gray; N: blue; O: red; Tb: emerald green.

Table S6 Interaction Energy (E_{int}) between ^{tBu}**1Tb′**/^{Me}**1Tb′** Units and (*R*)-**L$_{NH2}$** to Form ^{tBu}**1Tb**/(*R*)-**L$_{NH2}$** and ^{Me}**1Tb**/(*R*)-**L$_{NH2}$** Calculated at the DFT/B3LYP-D3BJ Level (ECP54MWB (Tb)/6-31G(d) (C, H, N, O), in THF (SAS))

	Δ-^{tBu}**1Tb**/(*R*)-**L$_{NH2}$**	*Δ*-^{Me}**1Tb**/(*R*)-**L$_{NH2}$**	*Λ*-^{tBu}**1Tb**/(*R*)-**L$_{NH2}$**	*Λ*-^{Me}**1Tb**/(*R*)-**L$_{NH2}$**
E /kcal mol^{-1}	−1,524,550.84	−1,302,497.32	−1,524,550.68	−1,302,497.64
E_{Tb} /kcal mol^{-1}	−1,294,690.94	−1,072,640.40	−1,294,690.41	−1,072,640.41
E_{NH2} /kcal mol^{-1}	−229,835.82	−229,836.24	−229,835.65	−229,836.28
E_{int} /kcal mol^{-1}	−24.07	−20.68	−24.62	−20.96
ΔE_{int} /kcal mol^{-1}	−3.40		−3.67	

E: Total energy of optimized structure of ^{tBu}**1Tb**/(*R*)-**L$_{NH2}$** and ^{Me}**1Tb**/(*R*)-**L$_{NH2}$**

E_{Tb}: Single-point calculated energy of ^{tBu}**1Tb′**/^{Me}**1Tb′**

E_{NH2}: Single-point calculated energy of (*R*)-**L$_{NH2}$**

$E_{int} = E - (E_{Tb} + E_{NH2})$

ΔE_{int}: Difference in interaction energies between ^{tBu}**1Tb**/(*R*)-**L$_{NH2}$** and ^{Me}**1Tb**/(*R*)-**L$_{NH2}$**

Table S7 Interaction Energy (E_{int}) between ^{tBu}**1Tb′**/^{Me}**1Tb′** Units and (*S*)-**L$_{NH2}$** to Form ^{tBu}**1Tb**/(*S*)-**L$_{NH2}$** and ^{Me}**1Tb**/(*S*)-**L$_{NH2}$** Calculated at the DFT/B3LYP-D3BJ Level (ECP54MWB (Tb)/6-31G(d) (C, H, N, O), in THF (SAS))

	Δ-^{tBu}**1Tb**/(*S*)-**L$_{NH2}$**	*Δ*-^{Me}**1Tb**/(*S*)-**L$_{NH2}$**	*Λ*-^{tBu}**1Tb**/(*S*)-**L$_{NH2}$**	*Λ*-^{Me}**1Tb**/(*S*)-**L$_{NH2}$**
E /kcal mol^{-1}	−1,524,550.69	−1,302,497.65	−1,524,550.89	−1,302,497.32
E_{Tb} /kcal mol^{-1}	−1,294,690.46	−1,072,640.36	−1,294,690.95	−1,072,640.39
E_{NH2} /kcal mol^{-1}	−229,835.65	−229,836.33	−229,835.83	−229,836.24
E_{int} /kcal mol^{-1}	−24.59	−20.95	−24.11	−20.68
ΔE_{int} /kcal mol^{-1}	−3.63		−3.42	

E: Total energy of optimized structure of ^{tBu}**1Tb**/(*S*)-**L$_{NH2}$** and ^{Me}**1Tb**/(*S*)-**L$_{NH2}$**

E_{Tb}: Single-point calculated energy of ^{tBu}**1Tb′**/^{Me}**1Tb′**

E_{NH2}: Single-point calculated energy of (*S*)-**L$_{NH2}$**

$E_{int} = E - (E_{Tb} + E_{NH2})$

ΔE_{int}: Difference in interaction energies between ^{tBu}**1Tb**/(*S*)-**L$_{NH2}$** and ^{Me}**1Tb**/(*S*)-**L$_{NH2}$**

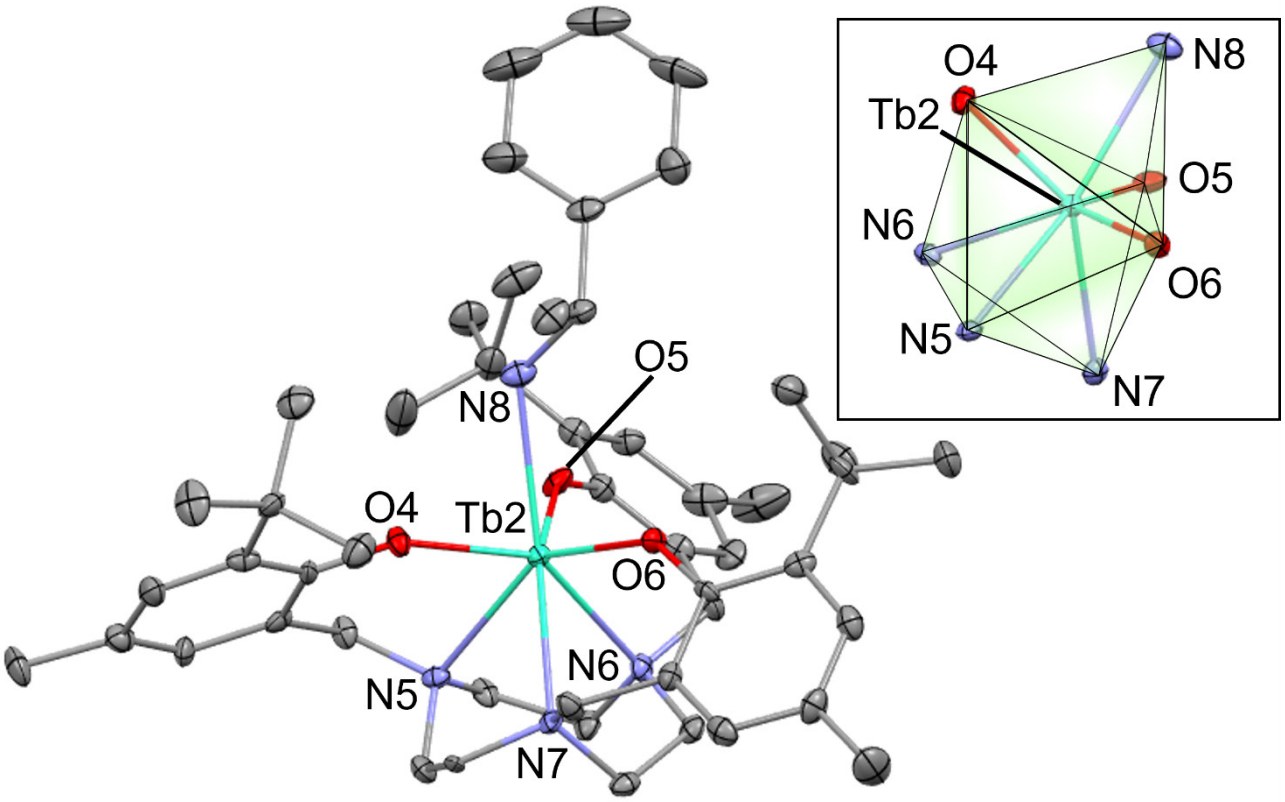

Fig. S14 ORTEP drawing of Tb complex $^{t\mathrm{Bu}}\mathbf{1}_{\mathbf{Tb}}$/(*R*)-$\mathbf{L}_{\mathbf{NH2}}$ (*Δ*-isomer, one of the four independent molecules in the crystals, at 123 K) with ellipsoids drawn at 50% probability. Hydrogen atoms and co-crystalized free (*R*)-$\mathbf{L}_{\mathbf{NH2}}$ are omitted for clarity. Selected bond lengths [Å] and angles [deg]: Tb2–N5 = 2.564(5), Tb2–N6 = 2.566(5), Tb2–N7 = 2.575(5), Tb2–N8 = 2.608(3), Tb2–O4 = 2.176(4), Tb2–O5 = 2.225(4), Tb2–O6 = 2.208(4), O4–Tb2–N8 = 75.90(14), O5–Tb2–N8 = 70.55(13), and O6–Tb2–N8 = 84.10(12). Inset: Coordination polyhedron of Tb^{3+} in $^{t\mathrm{Bu}}\mathbf{1}_{\mathbf{Tb}}$/(*R*)-$\mathbf{L}_{\mathbf{NH2}}$.

References

1. C. A. Barta, S. R. Bayly, P. W. Read, B. O. Patrick, R. C. Thompson and C. Orvig, *Inorg. Chem.*, 2008, **47**, 2280–2293.
2. H. Nakai, T. Goto, K. Kitagawa, K. Nonaka, T. Matsumoto and S. Ogo, *Chem. Commun.*, 2014, **50**, 15737–15739.
3. A. V. Nizovtsev, A. Scheurer, B. Kosog, F. W. Heinemann and K. Meyer, *Eur. J. Inorg. Chem.*, 2013, 2538–2548.
4. P. R. Sultane, T. B. Mete and R. G. Bhat, *Org. Biomol. Chem.*, 2014, **12**, 261–264.
5. G. M. Sheldrick, *Acta Cryst.*, 2015, **A71**, 3–8.
6. G. M. Sheldrick, *Acta Cryst.*, 2015, **C71**, 3–8.
7. O. V. Dolomanov, L. J. Bourhis, R. J. Gildea, J. A. K. Howard and H. Puschmann, *J. Appl. Cryst.*, 2009, **42**, 339–341.
8. K. Suzuki, A. Kobayashi, S. Kaneko, K. Takehira, T. Yoshihara, H. Ishida, Y. Shiina, S. Oishi and S. Tobita, *Phys. Chem. Chem. Phys.*, 2009, **11**, 9850–9860.
9. A. M. Brouwer, *Pure Appl. Chem.*, 2011, **83**, 2213–2228.
10. F. Zinna and L. Di Bari, *Chirality*, 2015, **27**, 1–13.
11. L. Arrico, L. Di Bari and F. Zinna, *Chem. Eur. J.*, 2021, **27**, 2920–2934.
12. (a) S. Grimme, J. Antony, S. Ehrlich and H. Krieg, *J. Chem. Phys.*, 2010, **132**, 154104. (b) S. Grimme, *Wiley Interdiscip. Rev. Comput. Mol. Sci.*, 2011, **1**, 211–228.
13. (a) A. D. Becke, *J. Chem. Phys.*, 1993, **98**, 1372–1377. (b) C. Lee, W. Yang and R. G. Parr, *Phys. Rev. B*, 1988, **37**, 785–789.
14. M. Dolg, H. Stoll, A. Savin and H. Preuss, *Theor. Chim. Acta*, 1989, **75**, 173–194.
15. W. J. Hehre, R. Ditchfield and J. A. Pople, *J. Chem. Phys.*, 1972, **56**, 2257–2261.
16. A. V. Marenich, C. J. Cramer and D. G. Truhlar, *J. Phys. Chem. B*, 2009, **113**, 6378–6396.
17. B. Marten, K. Kim, C. Cortis, R. A. Friesner, R. B. Murphy, M. N. Ringnalda, D. Sitkoff and B. Honig, *J. Phys. Chem.*, 1996, **100**, 11775–11788.
18. M. J. Frisch, G. W. Trucks, H. B. Schlegel, G. E. Scuseria, M. A. Robb, J. R. Cheeseman, G. Scalmani, V. Barone, G. A. Petersson, H. Nakatsuji, X. Li, M. Caricato, A. V. Marenich, J. Bloino, B. G. Janesko, R. Gomperts, B. Mennucci, H. P. Hratchian, J. V. Ortiz, A. F. Izmaylov, J. L. Sonnenberg, D. Williams-Young, F. Ding, F. Lipparini, F. Egidi, J. Goings, B. Peng, A. Petrone, T. Henderson, D. Ranasinghe, V. G. Zakrzewski, J. Gao, N. Rega, G. Zheng, W. Liang, M. Hada, M. Ehara, K. Toyota, R. Fukuda, J. Hasegawa, M. Ishida, T. Nakajima, Y. Honda, O. Kitao, H. Nakai, T. Vreven, K. Throssell, J. A. Montgomery, Jr., J. E. Peralta, F. Ogliaro, M. J. Bearpark, J. J. Heyd, E. N. Brothers, K. N. Kudin, V. N. Staroverov, T. A. Keith, R. Kobayashi, J. Normand, K. Raghavachari, A. P. Rendell, J. C. Burant, S. S. Iyengar, J. Tomasi, M. Cossi, J. M. Millam, M. Klene, C. Adamo, R. Cammi, J. W. Ochterski, R. L. Martin, K. Morokuma, O. Farkas, J. B. Foresman and D. J. Fox, *Gaussian 16*, Revision A.03, Gaussian, Inc., Wallingford CT, 2016, and *Gaussian 16*, Revision C.01 and C.02, Gaussian, Inc., Wallingford CT, 2019.
19. R. Dennington, T. A. Keith and J. M. Millam, *GaussView*, Version 6.0.16, Semichem Inc., Shawnee Mission, KS, 2016.
20. M. Llunell, D. Casanova, J. Cirera, P. Alemany and S. Alvarez, *SHAPE*, Version 2.1, Barcelona, 2013.